Evolution of volatility and composition in sesquiterpene-mixed and α-pinene secondary organic aerosol particles during isothermal evaporation

Zijun Li[1], Angela Buchholz[1, *], Arttu Ylisirniö[1], Luis Barreira[1,2], Liqing Hao[1], Siegfried Schobesberger[1], Taina Yli-Juuti[1], Annele Virtanen[1, *]

[1]Department of Applied Physics, University of Eastern Finland, Kuopio, Finland

[2]Atmospheric Composition Research, Finnish Meteorological Institute, Helsinki, Finland

Correspondence to: Angela Buchholz (angela.buchholz@uef.fi), and Annele Virtanen (annele.virtanen@uef.fi)

Abstract. Efforts have been spent on investigating the isothermal evaporation of α-pinene SOA particles at ranges of conditions and decoupling the impacts of viscosity and volatility on evaporation. However, little is known about the evaporation behavior of SOA particles from biogenic organic compounds other than α-pinene. In this study, we investigated the isothermal evaporation behavior of α-pinene and sesquiterpene mixture (SQTmix) SOA particles under a series of relative humidity (RH) conditions. With a set of in-situ instruments, we monitored the evolution of particle size, volatility, and composition during evaporation. Our finding demonstrates that the SQTmix SOA particles evaporated slower than the α-pinene ones at any set of RH (expressed with the volume fraction remaining (VFR)), which is primarily due to their lower volatility and possibly aided by higher viscosity under dry conditions. We further applied positive matrix factorization (PMF) to thermal desorption data containing volatility and composition information. Analyzing the net change ratios (NCRs) of each PMF-resolved factor, we can quantitatively compare how each sample factor evolves with increasing evaporation time/RH. When sufficient particulate water content was present in either SOA system, the most volatile sample factor was primarily lost via evaporation, and changes in other sample factors were mainly governed by aqueous-phase processes. The evolution of each sample factor of SQTmix SOA particles was controlled by a single type of process, whereas for α-pinene SOA particles it was regulated by multiple processes. As indicated by the coevolution of VFR and NCR, the effect of aqueous-phase processes could vary from one to another according to particle type, sample factors, and evaporation timescale.

1 Introduction

Atmospheric oxidation of volatile organic compounds (VOCs) can lead to a complex mixture of condensable organic vapors spanning ranges of functionalities and structures, and hence volatilities (Hallquist et al., 2009). Parts of these organics contribute to the mass concentration of secondary organic aerosol (SOA) particles. Gas-particle partitioning is a dynamic process of importance, influencing the composition in the gas and particle phase as well as the atmospheric lifetime of SOA. For a long time, gas-particle partitioning has been considered as a near-instantaneous process (Odum et al., 1996; Donahue et al., 2006), under the assumptions that SOA particles consist mainly of intermediate/semi-volatile compounds and exists in a liquid state. Recent measurements suggest that SOA particles consist of large amounts of organic compounds with low or extremely low volatility

(Cappa and Jimenez, 2010; Ehn et al., 2014; Mohr et al., 2019) and that particles can adopt viscous semisolid or amorphous solid states (Virtanen et al., 2010; Pajunoja et al., 2013; Zhang et al., 2015). All this emerging evidence challenges the abovementioned assumptions, which underlie the treatment of SOA via the partitioning theory. When volatilities of organic compounds range from intermediate to extremely low volatile (Donahue et al., 2012), the equilibration timescales of phase partitioning span from seconds to hours in liquid particles (Shiraiwa and Seinfeld, 2012). In viscous particles, bulk diffusion limitations can increase equilibration timescales to the order of years (Li and Shiraiwa, 2019).

Monoterpenes ($C_{10}H_{16}$) are the most abundant terpene emissions in boreal forests (Tarvainen et al., 2007; Bäck et al., 2012), driving SOA formation and growth in the atmosphere (O'Dowd et al., 2002; Jokinen et al., 2015). As the most representative monoterpene, α-pinene has been widely used to generate SOA as a proxy for boreal forest SOA. SOA yield studies using environmental chambers have suggested that α-pinene SOA particles are dominated by semi-volatile organic compounds (Pathak et al., 2007; Shilling et al., 2008). But multiple studies which investigated the isothermal evaporation of α-pinene SOA particles for a range of relative humidity (RH) consistently demonstrated that SOA particles do not evaporate as rapidly as expected for semi-volatile organic mixtures (Vaden et al., 2011; Wilson et al., 2014; Yli-Juuti et al., 2017; D'Ambro et al., 2018). These findings suggest the importance of unaccounted low-volatility organic compounds, particle phase reactions, and viscous phase states (Vaden et al., 2011; Wilson et al., 2014; Yli-Juuti et al., 2017; D'Ambro et al., 2018). While volatility distributions of organic compounds mainly determine the extent to which particles evaporate at high RH, diffusion limitations attributed to particle viscosity significantly hinder particle evaporation under dry conditions. Recent studies have also explored the oxidation and temperature dependence of the evaporation of α-pinene derived SOA particles. For instance, increasing the oxygen to carbon ratio (O:C) of the initial particles reduces the particle evaporation rate and possibly induces aqueous-phase processes which form low volatility compounds especially for highly oxidized SOA particles (Buchholz et al., 2019). Decreasing temperature can suppress particle evaporation by lowering the saturation vapor concentrations (C*) of the SOA compounds and/or increasing particle bulk viscosity (Shiraiwa et al., 2017; Li et al., 2019).

Efforts have been spent on investigating the evaporation of α-pinene SOA particles, but the diversity of VOC emissions from trees and the complexity of particulate constituents complicate the description of organic vapor partitioning in boreal forests. Branch enclosure measurements with boreal tree species have revealed that VOC emission profiles vary in terpene species and ratios, dependent on seasons (Hakola et al., 2017) or degrees of abiotic/biotic stress (Zhao et al., 2017a; Kari et al., 2019). Laboratory studies have shown that compared to α-pinene derived SOA particles, those derived from oxidizing sesquiterpenes ($C_{15}H_{24}$) or actual (stressed) Scots pine emissions feature distinct properties, in terms of mass yield, volatility, and molecular composition (Faiola et al., 2018; Ylisirniö et al., 2020). Given these observations, it is necessary to investigate the evaporation behavior of SOA particles derived from terpene precursors other than α-pinene and even from real plant emissions. Current measurements have identified that large amounts of farnesenes and bisabolenes are emitted from boreal tree species (Hakola et al., 2017; Danielsson et al., 2019) and that their derived SOA are of potential climate significance by influencing cloud formation (Mentel et al., 2013; Zhao et al., 2017a).

To facilitate a better understanding of biogenic organic vapor partitioning in boreal forests, α-pinene and a sesquiterpene mixture were chosen as precursors to generate two different types of biogenic SOA particles for isothermal evaporation under a range of RH conditions at room temperature. The mixture consists of farnesenes and bisabolenes, which are acyclic and monocyclic sesquiterpenes, respectively. The aim of this study is to compare the evaporation behavior of sesquiterpene derived SOA to that of

α–pinene derived SOA. For this, both the particle size changes as well as particle composition evolution were measured, and their differences and similarities will be discussed.

2 Methods

2.1 Experimental setup

Two different types of biogenic SOA particles were generated in a 13 L oxidation flow reactor (OFR) (Kang et al., 2007; Lambe et al., 2011) for isothermal evaporation experiments taking place at a wide range of RH at 25 °C. The experimental setup and procedure were similar to our previous evaporation studies (Yli-Juuti et al., 2017; Buchholz et al., 2019; Li et al., 2019) and a detailed description of our experimental setup can be found in the Supplement. Briefly, the experimental sequence consisted of biogenic SOA production, followed by particle size selection with simultaneous dilution of the gas phase, and humidity-controlled isothermal particle evaporation.

Either α-pinene (Sigma-Aldrich, 98%) or a sesquiterpene mixture (Sigma-Aldrich, mixture of isomers) was introduced into a heated N_2 flow with a syringe pump system (Kari et al., 2018). Farnesene isomers (40%, acyclic) and bisabolene isomers (40%, monocyclic) are the two dominant species in the mixture of sesquiterpenes, followed by other unidentified sesquiterpenes (Ylisirniö et al., 2020). The VOC-containing flow was then mixed with a humidified flow of N_2 and O_3. Overall, 5 L min^{-1} of total flow containing VOCs (254 − 261 ppb) and O_3 (13.01 – 13.40 ppm) with RH of 41% − 44% was introduced into the OFR for photooxidation at controlled temperature (~25 °C). Under the illumination of 254-nm UV lamps, hydroxyl radicals (OH) were produced from the reaction of water vapor with O (^{1}D) which was generated from photolysis of O_3. We produced α-pinene and sesquiterpene mixture (SQTmix) SOA with comparable oxidation conditions. The OH exposure ranges from 0.9 to 2.6×10^{11} molec cm^{-3} as calculated with the OFR model (Peng et al., 2015; Peng et al., 2016) which takes the external OH reactivity into account. The elemental composition of SOA particles was characterized by a high-resolution time-of-flight aerosol mass spectrometer (HR-ToF-AMS, Aerodyne Research Inc.). It should be noted that rather than by pure photooxidation, SOA was formed via both ozonolysis and photooxidation reactions, as O_3 levels of over 1 ppm were used. For all evaporation experiments of one SOA system, the aerosol mass concertation in the OFR was very similar. Assuming a particle density of 1.4 g cm^{-3}, the mass concertation of polydisperse α-pinene and SQTmix SOA from the OFR was estimated to be 399 ± 16 and 128 ± 16 μg m^{-3}, respectively. It has been found that compounds with C* of 0.1 μg m^{-3} and below dominate the SOA composition in a previous study using the same type of SOA (Ylisirniö et al., 2020). Even though the aerosol mass concentration in the OFR in our study is higher than the typical ambient level by one order of magnitude, such difference would not affect the gas-particle partitioning behavior of compounds with C* ≤ 0.1 μg m^{-3}. Experimental conditions and results for the SOA generation are summarized in Table S1.

The generated SOA was introduced into two parallel nanometer aerosol differential mobility analyzers (NanoDMA, model 3085, TSI) for particle size selection. The size selection process also diluted the organic vapors by 2 orders of magnitude with an open-loop sheath flow and thereby initiated particle evaporation. To vary the RH in samples, we humidified/dried the sheath flow of the NanoDMAs. The desired RH was set to one of three conditions: dry (< 7% RH), intermediate (40% RH), or high (80% RH). Eventually, a narrow distribution of SOA particles with 80 nm electrical mobility diameter was fed (i) to bypass lines with varying lengths for short evaporation measurements of up to 3 min, or (ii) to a 25 L stainless-steel residence time chambers (RTC) for intermediate evaporation measurements of up to 40 min with 10 min intervals, or (iii) to a 100 L RTC for long evaporation

measurements of up to 7.5 h with 1 h intervals. Prior to each particle evaporation experiment, the NanoDMAs, bypass tubing and
105   RTCs were flushed for at least 12 h with purified air at the desired RH of the following experiment.

2.2 Characterization of particle evaporation

Size changes of SOA particles due to evaporation were periodically monitored using a scanning mobility particle sizer (SMPS, model 3080, TSI). The extent of particle evaporation was evaluated in the terms of volume fraction remaining (VFR). Assuming particles are spherical, VFR was calculated as follows:

110   $$VFR = (\frac{D_{p,t}}{D_{p,0}})^3 , \tag{1}$$

where $D_{p,0}$ and $D_{p,t}$ are the particle sizes measured at the start (i.e., as selected by the NanoDMAs) and after time t of evaporation, respectively. The time evolution of particle evaporation was illustrated by plotting VFR against residence time (t_R) in the bypass tubing or RTC, defined as "evapogram", as shown in Figure 1. The selected particle size was calibrated using dry ammonium sulfate particles.

115   The thermal desorption behavior and chemical composition of particle samples were characterized using a chemical ionization mass spectrometer (CIMS, Aerodyne Research Inc.) coupled with a custom-built Filter Inlet for Gases and AEROsols (FIGAERO) (Ylisirniö et al., 2021) using iodide-adduct ionization (Lopez-Hilfiker et al., 2014). The operation of FIGAERO-CIMS can be found in the Supplement. Particle samples were collected for analysis (i) right after size selection (fresh, avg. t_R = 0.25 h, due to 0.5-h collection times) and (ii) after isothermal evaporation in the RTC (RTC, avg. t_R = 4.25 h). After a 30 min sample collection,
120   the collected particles were gradually desorbed with a heated N_2 flow of which the temperature was firstly ramped from 25 °C to ~200 °C within 20 min (desorption period), and then maintained at above 190 °C for an additional 15 min (soak period) to evaporate any residual organics left on the filter. The relationship between the temperature of the maximum desorption signal (T_{max}) of a single compound and its C^* was calibrated against a set of polyethylene glycol compounds (PEG, PEG 4 – 8) (Ylisirniö et al., 2021) with known vapor pressures (Krieger et al., 2018). The desorption temperature (T_{desorp}) range is divided into three volatility
125   ranges (i.e. semi-volatile organic compounds (SVOC), low-volatility organic compounds (LVOC), and extremely low volatility organic compounds (ELVOC)) as defined by Donahue et al. (2012).

The desorption temperature-dependent change in the sum of the organic signals over the temperature range is referred to as sum thermogram, STG. The appearance of the STG depends on the number of molecules collected on the FIGAERO filter and the volatility distribution of the sample. We are interested in determining if some compounds in the particle phase are lost or produced
130   during isothermal evaporation. To be able to investigate this, we need to account for changes in STG due to different collected sample mass and the isothermal evaporation. As it was not possible to determine the collected sample mass independently, we normalize the *STG(T)* with the total ion signal of each sample (N_{Tot}):

$$STG_N(T) = \frac{STG(T)}{N_{Tot}} . \tag{2}$$

In addition, we need to take into account how much material is expected to be removed from each individual particle due to the
135   isothermal evaporation. We assume that this removal is proportional to the change in the average VFR (VFR_{avg}) determined for the corresponding evaporation time and can be described with the removal factor ($f_{removal}$):

$$f_{removal} = \frac{VFR_{avg,RTC}}{VFR_{avg,fresh}} \cdot \alpha_{MW_{avg}}^{-1} \cdot \beta_{\rho_{avg}} , \tag{3}$$

where $VFR_{avg,fresh}$ and $VFR_{avg,RTC}$ are the average VFR during the FIGAERO sampling time at fresh and RTC evaporation stages. $\alpha_{MW_{avg}}$ is a parameter that describes the relative change in signal-weighted average molecular weight (MW) of the particle

140   bulk, $MW_{avg,RTC}/MW_{avg,fresh}$, and $\beta_{\rho_{avg}}$ is a parameter that captures the relative change in average particle density, ρ_{avg}, $\rho_{avg,RTC}/\rho_{avg,fresh}$. These two parameters convert the isothermal evaporation effect from the volumetric base to the molecular base.

We scale the normalized STG for the RTC sample ($STG_{N,RTC}(T)$) with $f_{removal}$ expressed in Eq. (3) to obtain the scaled STG for the RTC sample ($STG_{SC,RTC}(T)$):

145    $$STG_{SC,RTC}(T) = STG_{N,RTC}(T) \cdot \frac{VFR_{avg,RTC}}{VFR_{avg,fresh}} \cdot \alpha_{MW_{avg}}^{-1} \cdot \beta_{\rho_{avg}} \qquad (4)$$

A more detailed justification for this approach can be found in Appendix A. The values of $\alpha_{MW_{avg}}$ and $\beta_{\rho_{avg}}$ which were used for the calculation of $STG_{SC,RTC}(T)$ are given in Table C1. The ratio of VFR_{avg} is proportional to the material loss per particle, so is the resulting $STG_{SC,RTC}$. Hence $STG_{SC,RTC}(T)$ and $STG_{N,fresh}(T)$ can be compared quantitatively (Figure 2a), and the differences between them directly indicate if compounds with a certain desorption temperature are lost, produced or remained unchanged

150   during the isothermal evaporation. A similar approach can be used to investigate the evolution of PMF factors as explained in section 3.3.

Previously, T_{max} of the *STG(T)* was used to compare the overall volatility between particle samples (Ylisirniö et al., 2021). Here, the median desorption temperature (T_{50}, at which half of the cumulative *STG(T)* signal is reached) was used instead because it is a more general measure of the overall desorption behavior. Typically, these T_{50} values were higher than the T_{max} values, as most

155   signals were recorded at temperatures above T_{max}.

2.3 Deconvolution of FIGAERO-CIMS data set with Positive Matrix Factorization (PMF)

Since it was introduced by Paatero and Tapper (1994), PMF has been widely used to identify the contribution of different sources of trace compounds in ambient measurements (Ulbrich et al., 2009; Zhang et al., 2011; Yan et al., 2016). More recently, PMF has been adapted to analyze laboratory experiments for understanding chemical or physical aspects of systems of interest (Craven et

160   al., 2012; Zhao et al., 2017b; Buchholz et al., 2020). Regarding a FIGAERO-CIMS data set, PMF can separate sample signals from filter background and contamination. But more than that, this method can also identify multiple factors which represent not only isomeric compounds with different volatilities but also thermally decomposed products for each ion. Following the procedure outlined in Buchholz et al. (2020), constant error values (CNerror) which are derived from the noise at the end of thermogram scans were applied to all ions without further down-weighing. The PMF results were calculated using the PMF Evaluation Tool

165   (PET 3.05) with one to twelve factors and five fpeak rotations from -1 to +1. Additional information about the PMF analysis is described in the Supplement including justification for the selected solution. The PMF analysis was applied independently for each precursor to sets of FIGAERO-CIMS samples. Each set represents particles from one SOA precursor (α-pinene or SQTmix), which were collected at both evaporation stages (fresh and RTC) under dry and high RH conditions. Two types of blank measurements were added to the data set: (i) Measurements of the clean FIGAERO filter without sampling from the setup. These blanks

170   characterize the overall instrument background. (ii) Measurements of filters sampled directly after size selection for 30 min but with the DMA voltage set to 0 V. These blanks represent the background due to, e.g., adsorption of remaining gas-phase compounds onto the filter during the normal sample collection procedure.

3 Results and Discussion

3.1 Bulk volatility of SOA particles

3.1.1 Isothermal evaporation behaviour of SOA particles

The isothermal evaporation behavior of SOA particles is illustrated by the VFR as a function of t_R in Figure 1. The evaporation rate of dry SOA particles is the slowest, and the differences in sum (Figure 2) and factor thermograms (Figure 3 and Figure 4) between two evaporation stages are minor. The particle evaporation rate became faster with increasing RH for both SOA systems. When particulate water was present, the contribution of compounds in the SVOC range was reduced during fresh stages (Figure 2). As shown in previous studies (Yli-Juuti et al., 2017; Buchholz et al., 2019; Li et al., 2019; Zaveri et al., 2020), considerable kinetic limitations exist for the evaporation of volatile compounds in this type of dry SOA particles due to the substantially high viscosity. Particulate water reduces the viscosity and thus enhances particle evaporation with increasing RH. The comparable evaporation rates under intermediate and high RH conditions suggest that particle evaporation can be approximated as a liquid-like process for both conditions (i.e., at RH ≥ 40%), But in addition to this plasticizing effect, particulate water content may also induce aqueous-phase processes during isothermal evaporation (Buchholz et al., 2019; Petters et al., 2020). For the investigated SOA particles, we observed strong evidence of such processes under high RH conditions (RH = 80%). These are detailed in section 3.3.3. Quantifying the effects of particle viscosity and aqueous-phase processes on the SOA particle evaporation would require developing detailed processes models considering particle phase chemistry, which is not the primary focus of this study.

At any set RH, the evaporation rate of SQTmix SOA particles was slower than that of α-pinene ones, although both SOA were produced under comparable oxidation conditions. Such distinguishable evaporation patterns are most likely driven by (i) the distinct particulate volatility distributions jointly controlled by molecular weight and functionality, expressed by elemental composition as a proxy (Li et al., 2016), and/or (ii) the possible differences in particle bulk viscosities especially under dry conditions.

3.1.2 Thermal desorption behaviour of SOA particles

In Figure 2, the thermal desorption behavior of particle samples which were collected at fresh (avg. $t_R = 0.25$ h) and RTC (avg. $t_R = 4.25$ h) evaporation stages under dry (RH < 7%) and high RH (RH 80%) conditions are displayed as normalized $STG(T)$ ($STG_{N,fresh}(T)$, solid line) and scaled ones ($STG_{SC,RTC}(T)$, dashed line), respectively (Figure 2a, b). These two types of $STG(T)$ together are hereinafter referred to as STGs for simplicity unless otherwise specified. The corresponding T_{50} and VFR_{avg} are shown in Figure 2c, and the sampling periods for FIGAERO-CIMS thermograms are highlighted in colored areas in Figure 1. For each SOA system of interest, similar mass concentration of organic material after size selection was ensured for both dry and high RH conditions so that the volatility distribution of compounds in the condensed phase was not significantly affected. For the α-pinene case, the mass concentration of organic material after size selection was 4.47 and 5.31 μg cm^{-3} under dry and high RH conditions, respectively. For the SQTmix case, the corresponding values were 0.97 and 1.39 μg cm^{-3} under dry and high RH conditions.

Compared to the STGs of fresh samples, the STGs of the RTC samples shifted to higher T_{desorp} values with increases in T_{50}, regardless of the RH conditions. When examining the particle desorption profiles (i.e., STGs), we note that the removal of compounds which were thermally desorbed below 120 °C, and the corresponding changes in T_{50}, is more pronounced between

fresh and RTC samples at high RH as compared to that under the dry condition. Such difference in the changes of STGs between two RH conditions agrees with our observation of faster particle evaporation rates in the presence of water (see Figure 1).

Under dry conditions, a larger fraction of LVOC and ELVOC (collectively (E)LVOC) contributed to the STGs of SQTmix SOA particles, with higher values of T_{50} when compared to α-pinene particles (Figure 2a, c). Consistent with the changes in VFR_{avg} under dry conditions, relatively less increase in T_{50} and decrease in the STGs were observed in SQTmix SOA particles as well. On the other hand, similar STGs were observed for fresh samples at high RH, regardless of SOA particle type. According to the evaporation model simulations described in a previous study using a similar measurement setup (Li et al., 2019), a majority of I/SVOC is expected to evaporate rapidly from fresh particles during the first 8 – 30 min at high RH. It should be noted that during the same evaporation timescale (≤ 0.5h), the evaporation of (E)LVOC is expected to be negligible. Therefore, the VFR_{avg} (t_R = 0.25 h) is approximately determined by the ratio of (IVOC + SVOC)/(LVOC + ELVOC) in the initial particles. As the FIGAERO sampling periods last for 30 min, it follows that under high RH conditions, the fresh particles lost a significant fraction of the initially present I/SVOC during sample collection. Thus, the similarity in STGs between α-pinene and SQTmix SOA particles suggests that the (E)LVOC fraction in both SOA types has a similar volatility distribution and/or thermal desorption behavior. Note that this does not mean that the same types of compounds are present in the two different SOA types. For the same reason, the difference in T_{50} between two different types of fresh particles is less noticeable than the difference in VFR_{avg} at high RH (Figure 2c, solid circles).

3.2 PMF factors of SOA particles

Depending on the RH conditions or SOA precursors, the particle size and volatility appear to evolve differently during isothermal evaporation (Figure 1 and Figure 2). To better assess the compositional and volatility changes of the investigated SOA particles, we performed PMF analyses to deconvolute the thermal desorption profiles. Each derived factor constitutes a group of organic compounds with very similar "temporal" behavior. The PMF algorithm does not prescribe any meaning to the position of a value in the dataset, i.e., the T_{desorp} or desorption time values are only used to define the order of the data points. When volatility acts as the primary factor driving the composition change in the particles, compounds with similar desorption behavior correlate and are grouped into factors. In each factor, compounds of similar volatility evaporate in a similar manner during the isothermal evaporation so that the shape of the factor thermogram remains more or less constant between conditions. However, the occurrence of aqueous-phase processes may complicate the grouping of compounds especially for highly oxidized samples (Buchholz et al., 2020). Compounds with somewhat different volatility may no longer be separated but rather be grouped together due to how they are affected by the aqueous phase. This can create changes in the appearance of the factor thermogram (e.g., broadening) and possibly induce a non-negligible shift in T_{desorp} (≥ 15 °C) dependent on the extent of aqueous-phase processes. We provide more details about the behavior of the PMF algorithm, how compounds are grouped, and why the shape and characteristic T_{desorp} may change in the Supplement (see Section S1.2.3).

Two types of factors were identified. Factors occurring in particle samples but predominantly in filter blank measurements are defined as type B ("background") factors. The sum of type B factors showed similar absolute signal strength regardless of sample types. But while this contributed 10 - 60% to the total sum signal of the particle samples, it accounted for more than 80% of the total sum signal in filter blank samples. Type B factors displayed either nearly constant or very shallow factor thermograms. Factors which showed contributions in particle samples but not in filter blank samples were assumed to describe the collected particle sample and thus defined as type F ("sample") factors. In Buchholz et al. (2020), these sample factors were distinguished into ones

dominated by direct desorption of compounds (type V) and those dominated by products of thermal decomposition (type D). The careful analysis of the sample factors in this study showed that we could not make such a strict distinction. Thus, we decided to use the terms background factor (type B) and sample factor (type F) and point out which of the sample factors shows strong signs of thermal decomposition products.

PMF solutions with eight and ten factors were chosen for α-pinene and SQTmix SOA particles, respectively. In both PMF results, five factors are assigned as sample factors and the rest are considered background factors (i.e., type B factors). In the following discussion (Figure 3 and Figure 4), type B factors and the blank measurements are omitted. All mass spectral profiles and all factor thermograms of all samples of each data set can be found in Figure S3 and S4. Furthermore, ion distributions and bulk properties are visualized for each sample factor in the form of modified Kroll diagrams (Kroll et al., 2011) in Figure S10 and S11 by plotting the average carbon oxidation state (OSc) versus the carbon number (Cnum). By lumping ions with the same carbon number into a grid with a 0.2-interval on the y-axis of OSc, the issue of overlapping signals was avoided.

3.2.1 α-pinene SOA particles

In total, five sample factors (AF1 – 5, colored) were identified for α-pinene SOA particles as shown in Figure 3. For AF1 – AF4, average MW increased with higher T_{50} (i.e., lower volatility). While these factors were dominated by compounds with $C \leq 10$, as expected for a precursor composition of $C_{10}H_{16}$, additional amounts of compounds with $C > 10$ (i.e., dimers/oligomers) contributed to the total signal of AF3 and especially to that of AF4 (see also Figure S10a). With increasing T_{50} values, factors had longer carbon chain lengths and higher oxygen contents, as indicated by their average molecular composition. There was no clear association between OSc and T_{50} for factors AF1 - AF4, since the increase in carbon chain lengths is counterbalanced by the simultaneous addition of oxygen and hydrogen numbers. Therefore, the decrease in volatility of type V factors was mainly driven by the increase in average MW.

For AF5, its bulk properties and composition distribution (Figure 3 and Figure 5a) were closest to those of AF2 and AF3 with compounds with MW < 200 Da dominating their factor mass spectra. However, the thermal desorption behavior of AF5 was completely different with almost all of its signal occurring at $T_{desorp} > 100$ °C and a continuous increase with T_{desorp} until the soak period starts. Many of the compounds assigned to AF5 also showed contributions to other factors at lower T_{desorp} values. It is very unlikely that all these were isomeric compounds spanning 5 or more orders of magnitude in C* between the isomeric forms. It is much more probable that those compounds with small MW in AF5 were decomposition products of thermally unstable compounds with larger MW and lower volatility (D'Ambro et al., 2018; Schobesberger et al., 2018; Yang et al., 2021).

3.2.2 SQTmix SOA particles

In a similar way as for α-pinene SOA particles, five sample factors (i.e., SF1 – 5, colored) were identified for SQTmix SOA particles, as shown in Figure 4. For SF1 – SF4, lower volatilities characterized by higher T_{50} values again correlated with increasing average MW but not with average OSc. Furthermore, these factors mostly comprise compounds with $C \leq 15$ (Figure S10b), as expected for a precursor composition of $C_{15}H_{24}$. Due to the prevalence of acyclic structures in the C_{15} carbon skeletons of both farnesene and bisabolene (in particular exocyclic double bonds), the investigated SQTmix is more prone to undergo fragmentation, compared with those sesquiterpenes dominated by cyclic structures (e.g. β-caryophyllene) (Faiola et al., 2019). As these smaller fragments can undergo oligomerization reaction, compounds with $C < 15$ can also be oligomers (e.g., a C_{14} compound as

combination of two C_7 fragments). However, elucidating the detailed formation mechanisms of the observed compounds in SQTmix SOA particles goes beyond the scope of this study.

Like the AF5 factor in α-pinene SOA particles, the SF5 factor in SQTmix SOA particles contains mainly small compounds with MW < 200 Da despite displaying a continuous increase in signals at temperature above 100 °C (Figure 4). This, again, suggests that thermal decomposition is the main source process when compounds of SF5 were being desorbed from the FIGAERO filter. Consistently, the compositional profile of SF5 was also dominated by compounds with small carbon numbers (Figure 5b).

3.3 Evolution of PMF factors

As shown in the evapogram (Figure 1) and STGs (Figure 2), increasing RH enhanced evaporation rates of SOA particles and shifted particle volatility towards lower C*. These observed changes were caused not only by decreasing particle viscosities (Yli-Juuti et al., 2017; Buchholz et al., 2019; Li et al., 2019) but also possibly by aqueous-phase reactions, especially for highly oxidized particle samples (Buchholz et al., 2019). To further investigate how particulate water impacts particle evaporation processes here, we need to analyze how the factor volatility and the relative contribution of each factor to the signal of each sample change with isothermal evaporation and humidification. The volatility of each factor can be characterized by its characteristic T_{desorp} values (the 25th, 50th and 75th percentile desorption temperature) of factor thermogram. The 50th percentile is equivalent to T_{50} as used before, while the 25th and 75th ones indicate the width of a factor thermogram.

Due to different and uncertain amounts of sample mass, it is challenging to investigate changes in the contribution of factors between two evaporation stages by comparing their absolute signals. By normalizing the sum signal of a sample factor k to the total signal (excluding background factors) at the condition j ($F_{k,j}$), we can account for the difference in sample mass. Note that $F_{k,j}$ is not independent of the change in other factors. For instance, if the contribution of the most volatile factor decreases as it is removed by isothermal evaporation faster than other factors, the $F_{k,j}$ values of all other factors will increase. It would not be possible to separate such behavior from an absolute increase/decrease in the contribution of a factor (e.g., due to a formation/evaporation/decomposition process in the particles) based on the values of $F_{k,j}$ directly. To avoid this issue, we introduce the net change ratio (NCR) using the same rational as for the scaled STG (see section 2.2). We define the NCR as the ratio between the relative contribution of factor k at a given condition j ($F_{k,j}$) and that at the reference condition ($F_{k,ref}$) scaled by the changes caused by the overall evaporation of the particles:

$$NCR_{k,j} = \frac{F_{k,j}}{F_{k,ref}} \cdot \frac{VFR_{avg,j}}{VFR_{avg,ref}} \cdot \alpha_{MW_{avg,j}}^{-1} \cdot \beta_{\rho_{avg,j}} \qquad (5)$$

where $F_{k,j}$ and $F_{k,ref}$ are contribution of a sample factor k to the total signal (excluding background factors) measured by FIGAERO-CIMS at the condition j and reference condition, respectively. $VFR_{avg,j}$ and $VFR_{avg,ref}$ are the mean value of VFR retrieved from SMPS measurement at the condition j and reference condition. $a_{MW_{avg,j}}$ and $\beta_{\rho_{avg,j}}$ are similar to the $a_{MW_{avg}}$ and $\beta_{\rho_{avg}}$ parameters used in Eq. (4). It is not possible to capture the true initial state of particles, as particles start to evaporate directly after size selection. The dry and fresh condition exhibited the least amount of isothermal evaporation and thus was chosen as the reference case. More details about the derivation of Eq. (5) and the estimation of the parameters can be found in the Appendices B and C, respectively.

NCR represents the net effect of change in a factor, which is a combination of material loss (i.e., evaporation, chemical reactions) and production (i.e., chemical reactions), at a given condition as compared to the reference condition. If NCR is 1, the loss pathway counterbalances the production one, or no change occurs. NCR values significantly smaller than 1 (taking into account the possible uncertainties and limitations of the methodology, we consider $NCR_{k,j} < \frac{1}{2} NCR_{k,ref}$ being significantly smaller) suggests that the loss pathway outweighs the production one, and vice versa. There are two possible loss pathways: evaporation of compounds or transformation of compounds through chemical reactions. If the NCR is smaller than 1 and simultaneously decreases with increasing isothermal evaporation (i.e., decreasing VFR), it implies that the dominant loss mechanism may be evaporation. On the other hand, complex behavior of the NCR with increasing isothermal evaporation (e.g., a decrease followed by an increase) indicates that the main loss mechanism of the compounds is likely chemical transformation. When NCR is clearly larger than 1 (taking into account the possible uncertainties and limitations of the methodology, we consider $NCR_{k,j} > 2\ NCR_{k,ref}$ being significant larger), it implies that the compounds are produced in the particle phase. In addition to the trends in NCR values, the shape of the factor thermograms and their inferred C* values also give further insights into the possible production and loss mechanisms as discussed below.

3.3.1 SQTmix SOA particles

Consistent with the small change in VFR (< 12% in volume), the particle composition in dry SQTmix SOA particles barely changed (Figure 5, red colors), with negligible shifts only in the NCR of SF1. As seen in Figure 5, for the factors SF1, SF2 and SF4, the NCR decreased with decreasing VFR, implying the contribution of evaporation to the material loss. At high RH, SF1 and SF4 were no longer present after isothermal evaporation in the RTC.

As the range of C* assigned to the characteristic T_{desorp} of SF1 is high enough to enable significant evaporation during the experimental timescale of up to 4.25 h and its NCR exhibits a decreasing trend with evolving evaporation, we can conclude that the decrease in NCR of SF1 is primarily driven by evaporation. In this case, the particulate water mainly accelerated the evaporation as an effective plasticizer. The decrease of NCR for SF2 and SF4, which have volatilities in the LVOC and ELVOC range respectively, was even stronger than that of SF1 at high RH. This was surprising as compounds in that volatility range are not expected to evaporate significantly from particles within 4.5 h at room temperature (Li et al., 2019). Hence this observation indicates that in addition to evaporation, there was another loss mechanism (i.e., aqueous-phase process) driving the evolution of SF2 and SF4 under high RH conditions.

When investigating the factors SF3 and SF5, changes in their NCR were negligible under dry conditions, but significant increases in their NCR were seen at high RH (Figure 5). At the same time, we can see that both of these factors accounted for substantial amounts of the total particle composition at high RH (Figure 4). This clearly indicates that compounds in SF3 or SF5 were not only retained in particle phase due to their low C* values in the range of (E)LVOC, but also formed in the particle phase at high RH. These processes must be relatively fast as the changes in abundance and NCR were already clear at the fresh stage (i.e., within 0.25 h).

Except for SF1, all factors showed a distinct shift to higher values of characteristic T_{desorp} under high RH conditions as compared to dry conditions. This also indicates that the presence of water content has a more complex impact on the particle composition than simply enhancing the isothermal evaporation of volatile compounds. The correlations induced by the aqueous-phase processes are more important than the grouping solely by volatility class. I.e., compounds with a wider range of volatilities may be grouped

into a factor if they are produced by the same chemical process. We provide additional discussion about the possible reasons for the changes of the factor thermogram shapes in the Supplement (see section S1.2.3).

350   We will further elaborate on the possible reasons for these observed changes in NCR together with those described in the next section for α-pinene SOA particles in section 3.3.3.

3.3.2 α-pinene SOA particles

The response of STG to isothermal evaporation and humidification appeared very similar for α-pinene and SQTmix SOA particles (Figure 2a, b). The investigation of the NCR values of PMF factors revealed that, while the overall behavior is indeed similar,

355   there were also some distinct differences in chemical composition between these two types of SOA particles.

As expected from the isothermal evaporation measurements and the comparison of the STGs before and after isothermal evaporation in the RTC, α-pinene SOA particles showed very little change for the NCR under dry conditions (Figure 6, red colors). Under high RH conditions, AF1, AF2, and AF4 exhibited lower NCR values (NCR < 1) compared to the dry conditions (Figure 6). However, a continuous reduction in NCR with decreasing VFR (to the point that no contribution of the factor is detectable) was

360   only observed for AF1. Similar to the case of SF1, we concluded that the evolution of AF1 was primarily driven by the evaporation process controlled by its average C^* which lies in the volatility range between SVOC and LVOC.

The evolution of NCR with decreasing VFR was more complex for AF2 and AF4 as compared with that for AF1: their NCR values did not decrease with decreasing VFR but instead showed an increase with decreasing VFR at high RH. These observations imply that the aqueous-phase chemical transformation were the dominant processes affecting the evolution of AF2 and AF4 at high RH

365   instead of simple evaporation. Such chemical transformations could also cause the increases in the characteristic T_{desorp} and the factor thermogram width observed at high RH (Figure 3a and Figure 6a), in particular for AF2 with T_{50} increasing from 105 °C to 135 °C.

AF3 exhibited an NCR > 1 in the fresh case under high RH conditions, which means additional amounts of compounds grouped into that factor were formed in the presence of an aqueous phase in the particles. Note that many of the ions grouped into AF3 also

370   showed an increase in the absolute measured signal under high RH conditions after accounting for the different amount of collected sample mass on the filter. With longer isothermal evaporation time, NCR decreased for AF3, which means that some of the compounds grouped into AF3 must have evaporated from the particles or continued to react to form different products grouped into other factors. The change of the factor thermogram shape (i.e. loss of compounds with higher C^* and lower T_{desorp}) in Figure 3 together with a minor shift in the characteristic T_{desorp} in Figure 6 suggest that the removal due to evaporation is the more likely

375   explanation. Hence, the evolution of NCR of AF3 at high RH suggests complex behavior including the formation of compounds at the particle phase but also the loss of some compounds mainly by evaporation.

Negligible changes in NCR of AF5 alone indicates minor changes in composition during evaporation under dry or high RH conditions. In addition, when considering that AF5 is (mainly) in the ELVOC range (see Figure 3), the isothermal evaporation of compounds should not be significant in the experimental timescale of up to 4.5h (Li et al., 2019). But when investigating the factor

380   thermograms (Figure 3) in detail, the changes in the shape of the factor thermogram and T_{desop} (Figure 3) together implied that apart from evaporation, water driven aqueous-phase processes also affected at least some of the compounds with extremely low C^* which are grouped into AF5. Although both AF5 and SF5 were dominated by products of thermal decomposition, it does not indicate that their compositions are similar. While the mass spectra of AF5 was dominated by ions with Cnum from 7 to 10, major

ions in the mass spectra of SF5 tended to have Cnum of 6 or below (Figure S10). As these two factors originated from two different SOA systems, it is highly possible that they can behave differently against particulate water. It is also important to remember in this context that the products of any decomposition process may be similar or even identical, but they may stem from completely different parent compounds. Especially, very small fragments (e.g., oxalic acid or acetic acid) carry very little information about the original molecule they came from.

3.3.3 Interpretation of the evolution of NCRs

Overall, particulate water not only accelerates the evaporation of sample factors by reducing bulk diffusion limitations, but also alters the chemical composition of particles by inducing chemical aqueous-phase processes (e.g., hydrolysis or oligomerization). Accelerated evaporation primarily driven by the water plasticizing effect was observed for those sample factors with smallest average MW and highest volatility in both SOA systems (i.e., α-pinene: AF1 and SQTmix: SF1). On the other hand, changes in NCR together with changes in the absolute abundance and/or the characteristic T_{desorp} for other sample factors very likely suggest the presence of aqueous-phase processes that generally modify the composition and volatility of the (remaining) SOA particles.

The factors affected by chemical aqueous-phase processes can be classified as (i) "educt" factors with NCR < 1 and (ii) "product" factors with NCR > 1 under the same conditions. "Educt" factors contain water-labile compounds which are stable under dry conditions but undergo chemical reactions in the presence of water. Likely aqueous-phase reactions are the fragmentation (hydrolysis) of organic (hydro)peroxides (Krapf et al., 2016; Zhao et al., 2018; Qiu et al., 2019) or accretion reactions. Examples for these "educt" factors were SF2, SF4, AF2, and AF4. All these factors exhibited NCR values clearly < 1, while their volatilities were in the (E)LVOC range which makes a substantial isothermal evaporation within 0.25 h very unlikely.

The products of these aqueous-phase reactions will evaporate from the particle phase if their volatility is high enough (e.g., small fragments from fragmentation reactions). Products with sufficiently low volatility will remain in the particle phase and contribute to the "product" factors. Such compounds with sufficiently low volatility may be the larger fragments of fragmentation reactions, but the majority is likely formed from accretion reactions such as (i) non-oxidate reactions involving two or more carbonyls (i.e., (hemi)acetal formation, aldol condensation, and esterification), or (ii) reactions incorporating carbonyls and organic hydroperoxides (i.e., peroxy(hemi)acetal formation) (Kroll and Seinfeld, 2008; Herrmann et al., 2015). The predominant non-oxidative nature of these reactions is dictated by the fact that the average OSc of the particles does not increase under high RH conditions.

The "product" factors for SQTmix SOA particles (SF3 and SF5) were also identifiable by the fact that they almost have no contribution to the total signal under dry conditions. The comparable "product" factor for α-pinene SOA (AF3) already contributed to the particles under dry conditions and then showed an increase in contribution under high RH conditions. This behavior is probably linked to the SOA production inside the OFR which was at ~40% RH. For α-pinene SOA, compounds grouped into AF3 could be already produced inside the OFR either in the gas phase or by particle-phase processes. The absence/very small contribution of SF3 or SF5 under dry conditions indicates that the processes leading to their formation were too slow to produce significant amounts during the short residence time prior to the particle size selection.

Another difference between the two SOA types lies with the evolution of the "educt" and "product" factors in the RTC under high RH conditions. For SQTmix SOA particles, the evolution of the NCR values of all factors was monotonic (i.e., either increasing or decreasing with decreasing VFR). This may indicate that the underlying dominant process is either a removal or a production

process for each factor. It should be noted that multiple loss and production processes may coexist for a factor, especially at high RH where aqueous-phase processes may play a role. For instance, the removal of compounds grouped into the "educt" factor AF2 or AF4 via chemical reaction was dominant over any production process. But with increasing isothermal evaporation time at high RH, the balance between these processes shifted slightly, leading to a small increase in NCR. The balance between the removal and production of compounds may vary over time. This is probably the cause of the complex behavior of NCR values for AF2, AF3 and AF4 and may be coupled to the observed changes in factor thermogram shapes for these factors.

Although there are multiple studies of isothermal evaporation of α-pinene SOA particles, very few studies provide molecular information that is comparable to our approach. D'Ambro et al. (2018) conducted FIGAERO-CIMS measurements of particles that evaporated on the filter after collection. Although the α-pinene SOA particles in the study may not be directly comparable to the particles in our study, some of their findings share similarities with the interpretation of our PMF factors. For each ion, they explain the observed isothermal evaporation behavior with a model containing 3 components with different apparent volatility: (i) free monomers that evaporate from particles according to their C^* values, (ii) ELVOC compounds that do not evaporate from the particles at room temperature but decompose upon heating to be detected as the single ion, and (iii) reversible oligomers that decompose into the corresponding free monomers with time or heat. In our data set, many individual ions show contributions from multiple factors. AF1 and SF1 are predominantly containing compounds that behave like "free monomers". AF5 and SF5 are mostly ELVOC compounds that are detected as thermal decomposition products. The behavior described for "reversible oligomers" is in line with the complex behavior of the PMF factors which we associate with aqueous-phase processes. As D'Ambro et al. (2018) only applied their model investigation to particle evaporation at 50% RH and above, it is impossible to determine whether the particle phase processes affecting the reversible oligomers are linked to the presence of particulate water. Note that the approach of D'Ambro et al. (2018) deploys a ion-by-ion model fitting, while our PMF analysis inspects the behavior of all ions in the data set at once.

4. Atmospheric implications and conclusions

This isothermal evaporation study demonstrates that the SQTmix SOA particles evaporate slower than α-pinene ones. Additional compositional measurements with FIGAERO-CIMS enabled the separation of particulate constituents by their volatilities. By examining particle samples at two different evaporation stages (fresh vs. RTC), we observed relatively less changes in T_{50} and smaller decreases in the STGs of SQTmix SOA particles, in comparison with α-pinene SOA particles. This is in line with the observation of slower evaporation rates of SQTmix SOA particles during the isothermal evaporation. Compared to α-pinene SOA particles generated under comparable oxidation conditions, the overall less evaporation of SQTmix SOA can be attributed to its higher value of OSc which is consistent with its lower volatility and possibly higher viscosity.

To our knowledge, this is the first study investigating the volatility of SOA particles from a mixture of farnesene and bisabolene which are acyclic and monocyclic sesquiterpenes of atmospheric relevance. For α-pinene, multiple studies of isothermal evaporation at room temperature exist (Vaden et al., 2011; Wilson et al., 2014; Yli-Juuti et al., 2017; D'Ambro et al., 2018; Buchholz et al., 2019; Li et al., 2019; Zaveri et al., 2020; Pospisilova et al., 2021). However, even for this single precursor system, the formation conditions determine the isothermal evaporation behavior of the formed SOA and thus must be carefully considered when comparing different studies. The detailed composition of particles determines their volatility, viscosity, and behavior towards particulate water. Generally, particles containing increasing amounts of higher oxidized compounds will exhibit lower volatility

(Buchholz et al., 2019; Zaveri et al., 2020; Pospisilova et al., 2021), but may be more likely to be susceptible to aqueous-phase reactions (Buchholz et al., 2019). Unfortunately, not all previous studies provide an O/C, OSc value or similar proxy to estimate the degree of oxidation, which makes further comparisons difficult.

As the monoterpene with the largest emissions globally (Guenther et al., 2012), α-pinene has commonly served as a model precursor to generate biogenic SOA particles for laboratory studies. Results from these studies have been used to represent properties of many other terpene-derived SOA particles (excluding isoprene-derived SOA) in aerosol-climate models (O'Donnell et al., 2011; Gordon et al., 2016). Our study corroborates previous findings that sesquiterpene-derived particles are more viscous (Saukko et al., 2012), less hygroscopic (Pajunoja et al., 2015) and less volatile (Ylisirniö et al., 2020), compared to α-pinene SOA particles. Since the interplay of particle viscosity and volatility does impact the evaporation dynamics of particles, future studies should focus on particles derived from terpene precursors other than α-pinene to provide better parameterization to comprehensively constrain gas-to-particle partitioning behavior of different biogenic SOA particles.

We applied PMF to deconvolute the FIGAERO-CIMS data by grouping desorbed organic compounds into several sample factors. Such statistical analysis provides a useful simplification, compared to the full mass spectra, for describing how particle composition evolves during isothermal evaporation. In line with the minor change in the VFR under dry conditions, there was little difference in the particulate composition between fresh and RTC samples. On the other hand, the presence of particulate water dramatically altered the dry particle composition at high RH, likely by acting both as a plasticizer for bulk-surface diffusion and a catalyzer for aqueous-phase processes. In each SOA system, the most volatile factor was primarily lost via evaporation when high content of particulate water was present. As suggested by the change in NCR, the water-driven aqueous processes mainly governed the production and/or removal of other sample factors at high RH. Depending on the particle type, sample factors, and evaporation timescale, the effect of aqueous processes could be net production or net loss, which is indicated by the coevolution of particle VFR and factor NCR. While each sample factor of SQTmix SOA particles is largely controlled by a single type of process, the factors of α-pinene ones evolve according to the complex and time-dependent interplay of production and removal processes.

The observed aqueous-phase processes are not unique to SOA particles formed in the OFR. Prevalence of ether groups has been observed in ambient particles with high aerosol liquid water content, suggesting abundant formation of (hemi)acetals from carbonyls (Gilardoni et al., 2016; Ditto et al., 2020). Additionally, the prevalence of terpene-derived oligomers as well as carbon chain lengths have been found to decrease in cloud-water samples as compared to particle samples collected below cloud, indicating the possible presence of hydrolysis in cloud water (Boone et al., 2015). Although increasing evidence from laboratory and field observations have suggested the importance of aqueous-phase processes, such reactions are still underrepresented in the existing models because of a lack of fundamental knowledge (McNeill, 2015). While the aqueous-phase processes of simple, typically small carbonyl compounds have been well studied so far (De Haan et al., 2009; Schwier et al., 2010; Yasmeen et al., 2010; Li et al., 2011; Zhao et al., 2012; Zhao et al., 2013; Petters et al., 2020), more studies should investigate the processes involving complex and large molecules with multiple functional groups.

Appendix A. Scaled sum thermograms of RTC samples

To investigate the changes in volatility of SOA particles, we need to compare the number of ions at each desorption temperature between fresh (0.25 h, $N_{fresh}(T)$) and RTC (4.25 h, $N_{RTC}(T)$) samples collected by on the FIGAERO filter. The remaining fraction of all ions (RF) observed at a given temperature in each sample can be described as:

$$RF_{fresh}(T) = \frac{N_{fresh}(T)}{N_{0,fresh}(T)} \tag{A1}$$

$$RF_{RTC}(T) = \frac{N_{RTC}(T)}{N_{0,RTC}(T)} \tag{A2}$$

where $N_{0,fresh}(T)$ and $N_{0,RTC}(T)$ are the number of ions at each desorption temperature at each initial stage, i.e., before any isothermal evaporation occurred for the fresh and RTC samples, respectively. Note that $N_{0,fresh}(T)$ and $N_{0,RTC}(T)$ depend on the collected sample amount in each case.

The total remaining fraction of ions across the whole range of desorption temperatures (RF_{Tot}) is equal to:

$$RF_{Tot,fresh} = \frac{\sum_0^T N_{fresh}(T)}{\sum_0^T N_{0,fresh}(T)} = \frac{N_{Tot,fresh}}{N_{Tot,0,fresh}} \tag{A3}$$

$$RF_{Tot,RTC} = \frac{\sum_0^T N_{RTC}(T)}{\sum_0^T N_{0,RTC}(T)} = \frac{N_{Tot,RTC}}{N_{Tot,0,RTC}} \tag{A4}$$

where $N_{Tot,fresh}$ and $N_{Tot,RTC}$ are the sum of all ions over all desorption temperatures at the fresh and RTC stages. $N_{Tot,0,fresh}$ and $N_{Tot,0,RTC}$ are the same sums at the initial stage before any isothermal evaporation occurred for each sample.

In the absence of a reliable sensitivity calibration of the CIMS, the measured STG at a given desorption temperature ($STG_{fresh}(T)$ and $STG_{RTC}(T)$) is equivalent to the number of ions detected at this desorption temperature ($N_{fresh}(T)$ and $N_{RTC}(T)$). To account for different amounts of mass loadings on the FIGAERO filter, we normalize the measured STG with the total ion signal of each sample (N_{Tot}):

$$STG_{N,fresh}(T) = \frac{N_{fresh}(T)}{N_{Tot,fresh}} \tag{A5}$$

$$STG_{N,RTC}(T) = \frac{N_{RTC}(T)}{N_{Tot,RTC}} \tag{A6}$$

With Eq. (A2) − (A5), the expressions for the normalized STGs can be converted to:

$$STG_{N,fresh}(T) = \frac{N_{0,fresh}(T) \cdot RF_{fresh}(T)}{N_{Tot,0,fresh} \cdot RF_{Tot,fresh}} \tag{A7}$$

$$STG_{N,RTC}(T) = \frac{N_{0,RTC}(T) \cdot RF_{RTC}(T)}{N_{Tot,0,RTC} \cdot RF_{Tot,RTC}} \tag{A8}$$

Due to experimental limitations, different amounts of sample were collected in the fresh and RTC cases. Thus, the total signal at the corresponding initial stage is not equal either. However, the ratio between $N_0(T)$ and $N_{Tot,0}$ is independent of the amount of sample and can be expressed as:

$$k(T) = \frac{N_{0,fresh}(T)}{N_{Tot,0,fresh}} = \frac{N_{0,RTC}(T)}{N_{Tot,0,RTC}} \tag{A9}$$

Comparing the normalized STG is not equivalent to the direct comparison between $RF_{fresh}(T)$ and $RF_{RTC}(T)$, since $RF_{Tot,fresh}$ and $RF_{Tot,RTC}$ are not equal. We assume that the change in RF_{Tot} is determined by the isothermal evaporation, which is proportional to the change in the mean value of volume fraction remaining (VFR$_{avg}$). The VFR$_{avg}$ from the isothermal evaporation experiment must be converted to the molar scale first:

$$VFR_{avg,fresh} = \frac{N_{Tot,0,fresh} \cdot RF_{Tot,fresh}}{N_{Tot,0,fresh}} \cdot \frac{MW_{avg,fresh}}{MW_{avg,0}} \cdot \frac{\rho_{avg,0}}{\rho_{avg,fresh}}$$

$$= RF_{Tot,0,fresh} \cdot \frac{MW_{avg,fresh}}{MW_{avg,0}} \cdot \frac{\rho_{avg,0}}{\rho_{avg,fresh}} \tag{A10}$$

$$VFR_{avg,RTC} = \frac{N_{Tot,0,RTC} \cdot RF_{T,RTC}}{N_{Tot,0,RTC}} \cdot \frac{MW_{avg,RTC}}{MW_{avg,0}} \cdot \frac{\rho_{avg,0}}{\rho_{avg,RTC}}$$

$$= RF_{Tot,0,RTC} \cdot \frac{MW_{avg,RTC}}{MW_{avg,0}} \cdot \frac{\rho_{avg,0}}{\rho_{avg,RTC}} \tag{A11}$$

where $MW_{avg,fresh}$, $MW_{avg,RTC}$ and $MW_{avg,0}$ are the average molecular weight of the organic compounds and $\rho_{avg,fresh}$, $\rho_{avg,RTC}$ and $\rho_{avg,0}$ are the average particle density for the fresh, RTC, and initial stage, respectively.

Using Eq. (A10) and Eq. (A11), we can express the change in VFR$_{avg}$ between fresh and RTC samples as:

$$\frac{VFR_{avg,RTC}}{VFR_{avg,fresh}} = \frac{RF_{Tot,RTC}}{RF_{Tot,fresh}} \cdot \frac{MW_{avg,RTC}}{MW_{avg,fresh}} \cdot \frac{\rho_{avg,fresh}}{\rho_{avg,RTC}} \tag{A12}$$

Changes in the average molecular weight (MW_{avg}) of organic compounds and the average particle density (ρ_{avg}) during the isothermal evaporation can be expressed using $a_{MW_{avg}}$ and $\beta_{\rho_{avg}}$:

$$a_{MW_{avg}} = \frac{MW_{avg,RTC}}{MW_{avg,fresh}} \tag{A13}$$

$$\beta_{\rho_{avg}} = \frac{\rho_{avg,RTC}}{\rho_{avg,fresh}} \tag{A14}$$

Rearranging Eq. (A12) and using the definitions in Eq. (A13) and Eq. (A14), we can express the change in RF_{Tot} with the removal factor, $f_{removal}$:

$$f_{removal} = \frac{RF_{Tot,RTC}}{RF_{Tot,fresh}} = \frac{VFR_{avg,RTC}}{VFR_{avg,fresh}} \cdot \alpha_{MW_{avg}}^{-1} \cdot \beta_{\rho_{avg}} \tag{A15, Eq. (3) in main text}$$

To remove the term $RF_{Tot,RTC}$ in Eq. (A8), we multiple Eq. (A8) with Eq. (A15) to calculate the scaled STG ($STG_{SC,RTC}(T)$).

$$STG_{SC,RTC}(T) = STG_{N,RTC}(T) \cdot f_{removal} = \frac{N_{0,RTC}(T) \cdot RF_{RTC}(T)}{N_{Tot,0,RTC} \cdot RF_{Tot,fresh}} \tag{A16}$$

Eq. (A16) can be also expressed in the form in Eq. (A17) which is equivalent to Eq. (4) in the main text.

$$STG_{SC,RTC}(T) = STG_{N,RTC}(T) \cdot \frac{VFR_{avg,RTC}}{VFR_{avg,fresh}} \cdot \alpha_{MW_{avg}}^{-1} \cdot \beta_{\rho_{avg}} \tag{A17, Eq. (4) in main text}$$

Now we can rearrange Eq. (A7) and Eq. (A16) as follows:

$$RF_{fresh}(T) = \frac{N_{Tot,0,fresh} \cdot RF_{Tot,fresh}}{N_{0,fresh}(T)} \cdot STG_{N,fresh}(T) \tag{A18}$$

540 $$RF_{RTC}(T) = \frac{N_{Tot,0,RTC} \cdot RF_{Tot,fresh}}{N_{0,RTC}(T)} \cdot STG_{SC,RTC}(T) \tag{A19}$$

Using Eq. (A9), these can be simplified as:

$$RF_{fresh}(T) = \frac{RF_{Tot,fresh}}{k(T)} \cdot STG_{N,fresh}(T) \tag{A20}$$

$$RF_{RTC}(T) = \frac{RF_{Tot,fresh}}{k(T)} \cdot STG_{SC,RTC}(T) \tag{A21}$$

These two equations show that comparing $STG_{N,fresh}(T)$ with $STG_{SC,RTC}(T)$ is equivalent to the direct comparison between
545 $RF_{fresh}(T)$ and $RF_{RTC}(T)$.

Appendix B. Calculation of net change ratio (NCR) for each PMF sample factor

We want to investigate the evolution of each sample factor k during isothermal evaporation by comparing its contribution to the total particle composition at different conditions j (fresh vs RTC; dry vs. high RH). To account for different amounts of collective sample material on the FIGAERO filter, we normalize the measured sum of ions from a factor k ($N_{k,j}$) to the total ion signal of
550 each sample ($N_{Tot,j} = \sum_{k=1}^{5} N_{k,j}$) excluding the contribution of background factors. The contribution of a factor k ($F_{k,j}$) to each sample can be calculated as:

$$F_{k,j} = \frac{N_{k,j}}{\sum_{k=1}^{5} N_{k,j}} = \frac{N_{k,j}}{N_{Tot,j}} \tag{B1}$$

The remaining fraction of a sample ($RF_{Tot,j}$) can be calculated as follows:

$$RF_{Tot,j} = \frac{N_{Tot,j}}{N_{Tot,0,j}} \tag{B2}$$

555 where $N_{Tot,j}$ is the total ion signal of each sample and $N_{Tot,0,j}$ is the total ion signal at the initial state, i.e., before any isothermal evaporation occurred for the collected sample. It should be noted that the value of $N_{Tot,0,j}$ depends on the collected mass at each condition j.

In the same manner, the remaining fraction of a sample factor k at a condition j ($RF_{k,j}$) can be defined as:

$$RF_{k,j} = \frac{N_{k,j}}{N_{k,0,j}} \tag{B3}$$

560 where $N_{k,0,j}$ is the total ion signal of a factor k at the initial state. Similar to $N_{Tot,0,j}$, the value of $N_{k,0,j}$ also depends on the total sum signal of a sample k at a condition j.

Expressing $N_{Tot,j}$ and $N_{k,j}$ in Eq. (B1) with Eq. (B2) and Eq. (B3) yields:

$$F_{k,j} = \frac{N_{k,j}}{N_{Tot,0,j} \cdot RF_{T,j}} = \frac{N_{k,0,j} \cdot RF_{k,j}}{N_{Tot,0,j} \cdot RF_{Tot,j}} \tag{B4}$$

In the same manner as $\frac{N_0(T)}{N_{Tot,0}}$ expressed in Eq. (A9), the ratio between $N_{k,0}$ and N_{Tot} is also independent of the amount of sample

565 $$\frac{N_{k,0,j}}{N_{Tot,0,j}} = \frac{N_{k,0,ref}}{N_{Tot,0,ref}} \tag{B5}$$

It is not possible to capture the true initial state of particles, as particles start to evaporate directly after size selection. The dry and fresh condition exhibited the least amount of isothermal evaporation and thus was chosen as the reference case. By comparing $RF_{k,j}$ of the other sample with $RF_{k,ref}$, we could gain insights into the effect of increasing evaporation time and/or RH on each sample factor k. Here, we introduce the net change ratio (NCR) which is defined as the ratio between the remaining fraction of a sample factor k at a condition j ($RF_{k,j}$) and that at the reference condition ($RF_{k,ref}$). The principle of NCR is comparable to the scaling treatment applied to STG(T) of RTC samples (Appendix B). The NCR for a sample factor k at a condition j ($NCR_{k,j}$) can be expressed as follows:

$$NCR_{k,j} = \frac{RF_{k,j}}{RF_{k,ref}} \tag{B6}$$

Using Eq. (B4) and Eq. (B5), we rearrange Eq. (B6) and present $NCR_{k,j}$ as follows:

$$NCR_{k,j} = \frac{F_{k,j}}{F_{k,ref}} \cdot \frac{RF_{Tot,j}}{RF_{Tot,ref}} \tag{B7}$$

Note that the value of $NCR_{k,j}$ is not equivalent to the ratio of contribution of a factor k between the condition j and reference condition, since $RF_{Tot,j}$ is not equal to $RF_{Tot,ref}$. Similar to the scaled STG approach, the change in RF_{Tot} is assumed to be proportional to that in the VFR between two conditions (the condition j vs the reference condition). Similar to Eq. (A12), the ratio of RF_{Tot} between a condition j and reference condition can be solved as

$$\frac{RF_{Tot,j}}{RF_{Tot,ref}} = \frac{VFR_{avg,j}}{VFR_{avg,ref}} \cdot \frac{MW_{avg,ref}}{MW_{avg,j}} \cdot \frac{\rho_{avg,j}}{\rho_{avg,ref}} = \frac{VFR_{avg,j}}{VFR_{avg,ref}} \cdot \alpha^{-1}_{MW_{avg,j}} \cdot \beta_{\rho_{avg,j}} \tag{B8}$$

where $\alpha_{MW_{avg,j}}$ and $\beta_{\rho_{avg,j}}$ capture changes in signal-weighted molecular weight ($\frac{MW_{avg,j}}{MW_{avg,ref}}$) and particle density ($\frac{\rho_{avg,j}}{\rho_{avg,ref}}$) between a condition j and reference condition, respectively.

We replace $\frac{RF_{Tot,j}}{RF_{Tot,ref}}$ in Eq. (B7) with Eq. (B8) and then the $NCR_{k,j}$ of a factor k at a condition j can be expressed with the following equation:

$$NCR_{k,j} = \frac{F_{k,j}}{F_{k,ref}} \cdot \frac{VFR_{avg,j}}{VFR_{avg,ref}} \cdot \alpha^{-1}_{MW_{avg,j}} \cdot \beta_{\rho_{avg,j}} \tag{B9, Eq. (5) in main text}$$

Appendix C. Estimation of average molecular weight ($MW_{avg,j}$) and average particle density ($\rho_{avg,j}$) using PMF sample factors

For converting the VFR from the volumetric scale to the molar one, values of $MW_{avg,j}$ and $\rho_{avg,j}$ are needed at the condition j. For each sample factor k at a condition j, we calculate its signal-weighted average molar mass ($MW_{k,j}$) and then estimate its density ($\rho_{k,j}$) using its average O:C and H:C values (Kuwata et al., 2012). For those compounds grouped into factors AF5 and SF5, we are uncertain about the degree of thermal decomposition and that if the decomposition products can be detected by the instrument. In such case, we consider that either none or all of the compounds grouped into these two factors can undergo thermal decomposition during desorption and we also assume that at least 50% of these thermally labile compounds can be detected by the CIMS. Eventually, we calculate the $MW_{avg,j}$ and $\rho_{avg,j}$ as follows:

595    $MW_{avg,j} = \sum_{k=1}^{5} MW_{k,j} \cdot F_{k,j}$ (C1)

$\rho_{avg,j} = \sum_{k=1}^{5} \rho_{k,j} \cdot F_{k,j}$ (C2)

Using the $MW_{avg,j}$ and $\rho_{avg,j}$ at each condition j, we calculate the values of $a_{MW_{avg}}$ and $\beta_{\rho_{avg}}$ used for Eq. (A17) or those of $a_{MW_{avg,j}}$ and $\beta_{\rho_{avg,j}}$ used for Eq. (B9), as summarized in Table C1 and Table **C2**, respectively. Error bars of these parameters account for the uncertainty arising from the calculation of $MW_{k,j}$ and $\rho_{k,j}$ for factors AF5 and SF5.

600   **Table C1.** Ranges of parameters for scaling the normalized sum thermograms of RTC stages

SOA System	Fresh Condition	RTC Condition	$\frac{VFR_{avg,RTC}}{VFR_{avg,fresh}}$	α_{Mw}	$\beta_{\rho_{org}}$
α-pinene	Dry, Fresh	Dry, RTC	[0.85, 0.91]	[0.99, 1.01]	[1, 1]
	High RH, Fresh	High RH, RTC	[0.57, 0.73]	[1.02, 1.07]	[1.01, 1.01]
SQTmix	Dry, Fresh	Dry, RTC	[0.92, 0.95]	[1.01, 1.03]	[1, 1]
	High RH, Fresh	High RH, RTC	[0.73, 0.82]	[0.98, 1.03]	[1, 1.01]

Table C2. Ranges of parameters for calculating the net change ratio (NCR) for each PMF sample factor

SOA System	Ref. Condition	Condition j	$\frac{VFR_{avg,j}}{VFR_{avg,ref}}$	α_{Mw}	$\beta_{\rho_{org}}$
α-pinene	Dry, Fresh	Dry, RTC	[0.85, 0.91]	[0.99, 1.01]	[1, 1]
		High RH, Fresh	[0.77, 1.05]	[1.01, 1.07]	[0.99, 0.99]
		High RH, RTC	[0.56, 0.60]	[1.03, 1.14]	[1, 1]
SQTmix	Dry, Fresh	Dry, RTC	[0.92, 0.95]	[1.01, 1.03]	[1, 1]
		High RH, Fresh	[0.94, 1.07]	[0.98, 1.33]	[1.01, 1.01]
		High RH, RTC	[0.76, 0.80]	[1.00, 1.31]	[1.01, 1.01]

Data availability. The data set is available upon request from Annele Virtanen (annele.virtanen@uef.fi).

Supplement.

605 *Author contribution.* Z.L., A.B., T.Y.-J and A.V. designed the study. Z.L., A.B., A.Y., L.B., and L.H. carried out laboratory experiments. Z.L., A.B., S.S., T.Y.-J and A.V. performed data analysis and interpretation. Z.L., wrote the paper with contributions from all coauthors.

Competing interests. The authors declare that they have no conflict of interest.

Acknowledgements. This research was supported by the European Research Council (ERC StG QAPPA 335478), the Academy of
610 Finland Center of Excellence Program (decision 307331), the Academy of Finland (299544, 310682 and 317373), and the University of Eastern Finland Doctoral Program in Environmental Physics, Health and Biology (EPHB).

References

Boone, E. J., Laskin, A., Laskin, J., Wirth, C., Shepson, P. B., Stirm, B. H., and Pratt, K. A.: Aqueous processing of
615 atmospheric organic particles in cloud water collected via aircraft sampling, Environ. Sci. Technol., 49, 8523-8530,
2015.
Buchholz, A., Lambe, A. T., Ylisirniö, A., Li, Z., Tikkanen, O.-P., Faiola, C., Kari, E., Hao, L., Luoma, O., Huang,
W., Mohr, C., Worsnop, D. R., Nizkorodov, S. A., Yli-Juuti, T., Schobesberger, S., and Virtanen, A.: Insights into the
o: C-dependent mechanisms controlling the evaporation of α-pinene secondary organic aerosol particles, Atmos. Chem.
620 Phys., 19, 4061-4073, 2019.
Buchholz, A., Ylisirniö, A., Huang, W., Mohr, C., Canagaratna, M., Worsnop, D. R., Schobesberger, S., and Virtanen,
A.: Deconvolution of FIGAERO–CIMS thermal desorption profiles using positive matrix factorisation to identify
chemical and physical processes during particle evaporation, Atmos. Chem. Phys., 20, 7693-7716, 2020.
Bäck, J., Aalto, J., Henriksson, M., Hakola, H., He, Q., and Boy, M.: Chemodiversity of a scots pine stand and
625 implications for terpene air concentrations, Biogeosciences, 9, 689-702, 2012.
Cappa, C. D. and Jimenez, J. L.: Quantitative estimates of the volatility of ambient organic aerosol, Atmos. Chem.
Phys., 10, 5409-5424, 2010.
Craven, J., Yee, L., Ng, N., Canagaratna, M., Loza, C., Schilling, K., Yatavelli, R., Thornton, J., Ziemann, P., and
Flagan, R.: Analysis of secondary organic aerosol formation and aging using positive matrix factorization of high-
630 resolution aerosol mass spectra: Application to the dodecane low-NOx system, Atmos. Chem. Phys., 12, 11795-11817,
2012.
D'Ambro, E. L., Schobesberger, S., Zaveri, R. A., Shilling, J. E., Lee, B. H., Lopez-Hilfiker, F. D., Mohr, C., and
Thornton, J. A.: Isothermal evaporation of α-pinene ozonolysis SOA: Volatility, phase state, and oligomeric
composition, ACS Earth and Space Chemistry, 2, 1058-1067, 2018.
635 Danielsson, M., Zhaol, T., and Borg-Karlson, A. K.: Arthropod infestation sites and induced defence can be traced by
emission from single spruce needles, Arthropod-Plant Interactions, 13, 253-259, 2019.
De Haan, D. O., Corrigan, A. L., Tolbert, M. A., Jimenez, J. L., Wood, S. E., and Turley, J. J.: Secondary organic
aerosol formation by self-reactions of methylglyoxal and glyoxal in evaporating droplets, Environ. Sci. Technol., 43,
8184-8190, 2009.
640 Ditto, J. C., Joo, T., Slade, J. H., Shepson, P. B., Ng, N. L., and Gentner, D. R.: Nontargeted tandem mass spectrometry
analysis reveals diversity and variability in aerosol functional groups across multiple sites, seasons, and times of day,
Environmental Science & Technology Letters, 7, 60-69, 2020.
Donahue, N. M., Kroll, J. H., Pandis, S. N., and Robinson, A. L.: A two-dimensional volatility basis set – part 2:
Diagnostics of organic-aerosol evolution, Atmos. Chem. Phys., 12, 615-634, 2012.
645 Donahue, N. M., Robinson, A. L., Stanier, C. O., and Pandis, S. N.: Coupled partitioning, dilution, and chemical aging
of semivolatile organics, Environ. Sci. Technol., 40, 2635-2643, 2006.
Ehn, M., Thornton, J. A., Kleist, E., Sipila, M., Junninen, H., Pullinen, I., Springer, M., Rubach, F., Tillmann, R., Lee,
B., Lopez-Hilfiker, F., Andres, S., Acir, I. H., Rissanen, M., Jokinen, T., Schobesberger, S., Kangasluoma, J.,
Kontkanen, J., Nieminen, T., Kurten, T., Nielsen, L. B., Jorgensen, S., Kjaergaard, H. G., Canagaratna, M., Maso, M.
650 D., Berndt, T., Petaja, T., Wahner, A., Kerminen, V. M., Kulmala, M., Worsnop, D. R., Wildt, J., and Mentel, T. F.: A
large source of low-volatility secondary organic aerosol, Nature, 506, 476-479, 2014.
Faiola, C. L., Buchholz, A., Kari, E., Yli-Pirila, P., Holopainen, J. K., Kivimaenpaa, M., Miettinen, P., Worsnop, D.
R., Lehtinen, K. E. J., Guenther, A. B., and Virtanen, A.: Terpene composition complexity controls secondary organic
aerosol yields from scots pine volatile emissions, Sci. Rep., 8, 3053, 2018.
655 Faiola, C. L., Pullinen, I., Buchholz, A., Khalaj, F., Ylisirnio, A., Kari, E., Miettinen, P., Holopainen, J. K.,
Kivimaenpaa, M., Schobesberger, S., Yli-Juuti, T., and Virtanen, A.: Secondary organic aerosol formation from healthy
and aphid-stressed scots pine emissions, ACS Earth and Space Chemistry, 3, 1756-1772, 2019.
Gilardoni, S., Massoli, P., Paglione, M., Giulianelli, L., Carbone, C., Rinaldi, M., Decesari, S., Sandrini, S., Costabile,
F., Gobbi, G. P., Pietrogrande, M. C., Visentin, M., Scotto, F., Fuzzi, S., and Facchini, M. C.: Direct observation of
660 aqueous secondary organic aerosol from biomass-burning emissions, Proc. Natl. Acad. Sci. U. S. A., 113, 10013-10018,
2016.
Gordon, H., Sengupta, K., Rap, A., Duplissy, J., Frege, C., Williamson, C., Heinritzi, M., Simon, M., Yan, C., Almeida,
J., Trostl, J., Nieminen, T., Ortega, I. K., Wagner, R., Dunne, E. M., Adamov, A., Amorim, A., Bernhammer, A. K.,

Bianchi, F., Breitenlechner, M., Brilke, S., Chen, X., Craven, J. S., Dias, A., Ehrhart, S., Fischer, L., Flagan, R. C., Franchin, A., Fuchs, C., Guida, R., Hakala, J., Hoyle, C. R., Jokinen, T., Junninen, H., Kangasluoma, J., Kim, J., Kirkby, J., Krapf, M., Kurten, A., Laaksonen, A., Lehtipalo, K., Makhmutov, V., Mathot, S., Molteni, U., Monks, S. A., Onnela, A., Perakyla, O., Piel, F., Petaja, T., Praplan, A. P., Pringle, K. J., Richards, N. A., Rissanen, M. P., Rondo, L., Sarnela, N., Schobesberger, S., Scott, C. E., Seinfeld, J. H., Sharma, S., Sipila, M., Steiner, G., Stozhkov, Y., Stratmann, F., Tome, A., Virtanen, A., Vogel, A. L., Wagner, A. C., Wagner, P. E., Weingartner, E., Wimmer, D., Winkler, P. M., Ye, P., Zhang, X., Hansel, A., Dommen, J., Donahue, N. M., Worsnop, D. R., Baltensperger, U., Kulmala, M., Curtius, J., and Carslaw, K. S.: Reduced anthropogenic aerosol radiative forcing caused by biogenic new particle formation, Proc. Natl. Acad. Sci. U. S. A., 113, 12053-12058, 2016.

Guenther, A., Jiang, X., Heald, C. L., Sakulyanontvittaya, T., Duhl, T., Emmons, L., and Wang, X.: The model of emissions of gases and aerosols from nature version 2.1 (megan2. 1): An extended and updated framework for modeling biogenic emissions, Geoscientific Model Development, 5, 1471-1492, 2012.

Hakola, H., Tarvainen, V., Praplan, A. P., Jaars, K., Hemmila, M., Kulmala, M., Back, J., and Hellen, H.: Terpenoid and carbonyl emissions from norway spruce in finland during the growing season, Atmos. Chem. Phys., 17, 3357-3370, 2017.

Hallquist, M., Wenger, J. C., Baltensperger, U., Rudich, Y., Simpson, D., Claeys, M., Dommen, J., Donahue, N. M., George, C., Goldstein, A. H., Hamilton, J. F., Herrmann, H., Hoffmann, T., Iinuma, Y., Jang, M., Jenkin, M. E., Jimenez, J. L., Kiendler-Scharr, A., Maenhaut, W., McFiggans, G., Mentel, T. F., Monod, A., Prevot, A. S. H., Seinfeld, J. H., Surratt, J. D., Szmigielski, R., and Wildt, J.: The formation, properties and impact of secondary organic aerosol: Current and emerging issues, Atmos. Chem. Phys., 9, 5155-5236, 2009.

Herrmann, H., Schaefer, T., Tilgner, A., Styler, S. A., Weller, C., Teich, M., and Otto, T.: Tropospheric aqueous-phase chemistry: Kinetics, mechanisms, and its coupling to a changing gas phase, Chem. Rev., 115, 4259-4334, 2015.

Jokinen, T., Berndt, T., Makkonen, R., Kerminen, V. M., Junninen, H., Paasonen, P., Stratmann, F., Herrmann, H., Guenther, A. B., Worsnop, D. R., Kulmala, M., Ehn, M., and Sipila, M.: Production of extremely low volatile organic compounds from biogenic emissions: Measured yields and atmospheric implications, Proc. Natl. Acad. Sci. U. S. A., 112, 7123-7128, 2015.

Kang, E., Root, M. J., Toohey, D. W., and Brune, W. H.: Introducing the concept of potential aerosol mass (PAM), Atmos. Chem. Phys., 7, 5727-5744, 2007.

Kari, E., Faiola, C. L., Isokaanta, S., Miettinen, P., Yli-Pirila, P., Buchholz, A., Kivimaenpaa, M., Mikkonenn, S., Holopainen, J. K., and Virtanen, A.: Time-resolved characterization of biotic stress emissions from scots pines being fed upon by pine weevil by means of PTR-ToF-MS, Boreal Environ. Res., 24, 25-49, 2019.

Kari, E., Miettinen, P., Yli-Pirilä, P., Virtanen, A., and Faiola, C. L.: PTR-ToF-MS product ion distributions and humidity-dependence of biogenic volatile organic compounds, Int. J. Mass spectrom., 430, 87-97, 2018.

Krapf, M., El Haddad, I., Bruns, E. A., Molteni, U., Daellenbach, K. R., Prevot, A. S. H., Baltensperger, U., and Dommen, J.: Labile peroxides in secondary organic aerosol, Chem, 1, 603-616, 2016.

Krieger, U. K., Siegrist, F., Marcolli, C., Emanuelsson, E. U., Gøbel, F. M., Bilde, M., Marsh, A., Reid, J. P., Huisman, A. J., and Riipinen, I.: A reference data set for validating vapor pressure measurement techniques: Homologous series of polyethylene glycols, Atmos. Meas. Tech., 11, 49-63, 2018.

Kroll, J. H., Donahue, N. M., Jimenez, J. L., Kessler, S. H., Canagaratna, M. R., Wilson, K. R., Altieri, K. E., Mazzoleni, L. R., Wozniak, A. S., Bluhm, H., Mysak, E. R., Smith, J. D., Kolb, C. E., and Worsnop, D. R.: Carbon oxidation state as a metric for describing the chemistry of atmospheric organic aerosol, Nat. Chem, 3, 133-139, 2011.

Kroll, J. H. and Seinfeld, J. H.: Chemistry of secondary organic aerosol: Formation and evolution of low-volatility organics in the atmosphere, Atmos. Environ., 42, 3593-3624, 2008.

Kuwata, M., Zorn, S. R., and Martin, S. T.: Using elemental ratios to predict the density of organic material composed of carbon, hydrogen, and oxygen, Environ. Sci. Technol., 46, 787-794, 2012.

Lambe, A. T., Onasch, T. B., Massoli, P., Croasdale, D. R., Wright, J. P., Ahern, A. T., Williams, L. R., Worsnop, D. R., Brune, W. H., and Davidovits, P.: Laboratory studies of the chemical composition and cloud condensation nuclei (CCN) activity of secondary organic aerosol (SOA) and oxidized primary organic aerosol (OPOA), Atmos. Chem. Phys., 11, 8913-8928, 2011.

Li, Y., Poschl, U., and Shiraiwa, M.: Molecular corridors and parameterizations of volatility in the chemical evolution of organic aerosols, Atmos. Chem. Phys., 16, 3327-3344, 2016.

Li, Y. and Shiraiwa, M.: Timescales of secondary organic aerosols to reach equilibrium at various temperatures and relative humidities, Atmos. Chem. Phys., 19, 5959-5971, 2019.

Li, Z., Schwier, A. N., Sareen, N., and McNeill, V. F.: Reactive processing of formaldehyde and acetaldehyde in aqueous aerosol mimics: Surface tension depression and secondary organic products, Atmos. Chem. Phys., 11, 11617-11629, 2011.

720 Li, Z., Tikkanen, O.-P., Buchholz, A., Hao, L., Kari, E., Yli-Juuti, T., and Virtanen, A.: Effect of decreased temperature on the evaporation of α-pinene secondary organic aerosol particles, ACS Earth and Space Chemistry, 3, 2775-2785, 2019.

Lopez-Hilfiker, F. D., Mohr, C., Ehn, M., Rubach, F., Kleist, E., Wildt, J., Mentel, T. F., Lutz, A., Hallquist, M., Worsnop, D., and Thornton, J. A.: A novel method for online analysis of gas and particle composition: Description and

725 evaluation of a filter inlet for gases and aerosols (FIGAERO), Atmos. Meas. Tech., 7, 983-1001, 2014.

McNeill, V. F.: Aqueous organic chemistry in the atmosphere: Sources and chemical processing of organic aerosols, Environ. Sci. Technol., 49, 1237-1244, 2015.

Mentel, T. F., Kleist, E., Andres, S., Dal Maso, M., Hohaus, T., Kiendler-Scharr, A., Rudich, Y., Springer, M., Tillmann, R., Uerlings, R., Wahner, A., and Wildt, J.: Secondary aerosol formation from stress-induced biogenic emissions and

730 possible climate feedbacks, Atmos. Chem. Phys., 13, 8755-8770, 2013.

Mohr, C., Thornton, J. A., Heitto, A., Lopez-Hilfiker, F. D., Lutz, A., Riipinen, I., Hong, J., Donahue, N. M., Hallquist, M., Petaja, T., Kulmala, M., and Yli-Juuti, T.: Molecular identification of organic vapors driving atmospheric nanoparticle growth, Nat. Commun, 10, 4442, 2019.

O'Donnell, D., Tsigaridis, K., and Feichter, J.: Estimating the direct and indirect effects of secondary organic aerosols

735 using echam5-ham, Atmos. Chem. Phys., 11, 8635-8659, 2011.

O'Dowd, C. D., Aalto, P., Hmeri, K., Kulmala, M., and Hoffmann, T.: Aerosol formation: Atmospheric particles from organic vapours, Nature, 416, 497-498, 2002.

Odum, J. R., Hoffmann, T., Bowman, F., Collins, D., Flagan, R. C., and Seinfeld, J. H.: Gas/particle partitioning and secondary organic aerosol yields, Environ. Sci. Technol., 30, 2580-2585, 1996.

740 Paatero, P. and Tapper, U.: Positive matrix factorization: A non-negative factor model with optimal utilization of error estimates of data values, Environmetrics, 5, 111-126, 1994.

Pajunoja, A., Lambe, A. T., Hakala, J., Rastak, N., Cummings, M. J., Brogan, J. F., Hao, L. Q., Paramonov, M., Hong, J., Prisle, N. L., Malila, J., Romakkaniemi, S., Lehtinen, K. E. J., Laaksonen, A., Kulmala, M., Massoli, P., Onasch, T. B., Donahue, N. M., Riipinen, I., Davidovits, P., Worsnop, D. R., Petaja, T., and Virtanen, A.: Adsorptive uptake of

745 water by semisolid secondary organic aerosols, Geophys. Res. Lett., 42, 3063-3068, 2015.

Pajunoja, A., Malila, J., Hao, L., Joutsensaari, J., Lehtinen, K. E. J., and Virtanen, A.: Estimating the viscosity range of SOA particles based on their coalescence time, Aerosol Science and Technology, 48, i-iv, 2013.

Pathak, R., Presto, A., Lane, T., Stanier, C., Donahue, N., and Pandis, S.: Ozonolysis of α-pinene: Parameterization of secondary organic aerosol mass fraction, Atmos. Chem. Phys., 7, 3811-3821, 2007.

750 Peng, Z., Day, D. A., Ortega, A. M., Palm, B. B., Hu, W. W., Stark, H., Li, R., Tsigaridis, K., Brune, W. H., and Jimenez, J. L.: Non-OH chemistry in oxidation flow reactors for the study of atmospheric chemistry systematically examined by modeling, Atmos. Chem. Phys., 16, 4283-4305, 2016.

Peng, Z., Day, D. A., Stark, H., Li, R., Lee-Taylor, J., Palm, B. B., Brune, W. H., and Jimenez, J. L.: Hox radical chemistry in oxidation flow reactors with low-pressure mercury lamps systematically examined by modeling, Atmos.

755 Meas. Tech., 8, 4863-4890, 2015.

Petters, S. S., Hilditch, T. G., Tomaz, S., Miles, R. E. H., Reid, J. P., and Turpin, B. J.: Volatility change during droplet evaporation of pyruvic acid, ACS Earth and Space Chemistry, 4, 741-749, 2020.

Pospisilova, V., Bell, D. M., Lamkaddam, H., Bertrand, A., Wang, L., Bhattu, D., Zhou, X., Dommen, J., Prevot, A. S., and Baltensperger, U.: Photodegradation of α-pinene secondary organic aerosol dominated by moderately oxidized

760 molecules, Environ. Sci. Technol., 55, 6936-6943, 2021.

Qiu, J., Ishizuka, S., Tonokura, K., Colussi, A. J., and Enami, S.: Water dramatically accelerates the decomposition of alpha-hydroxyalkyl-hydroperoxides in aerosol particles, J. Phys. Chem. Lett., 10, 5748-5755, 2019.

Saukko, E., Lambe, A. T., Massoli, P., Koop, T., Wright, J. P., Croasdale, D. R., Pedernera, D. A., Onasch, T. B., Laaksonen, A., Davidovits, P., Worsnop, D. R., and Virtanen, A.: Humidity-dependent phase state of SOA particles

765 from biogenic and anthropogenic precursors, Atmos. Chem. Phys., 12, 7517-7529, 2012.

Schobesberger, S., D'Ambro, E. L., Lopez-Hilfiker, F. D., Mohr, C., and Thornton, J. A.: A model framework to retrieve thermodynamic and kinetic properties of organic aerosol from composition-resolved thermal desorption measurements, Atmos. Chem. Phys., 18, 14757-14785, 2018.

Schwier, A. N., Sareen, N., Mitroo, D., Shapiro, E. L., and McNeill, V. F.: Glyoxal-methylglyoxal cross-reactions in secondary organic aerosol formation, Environ. Sci. Technol., 44, 6174-6182, 2010.

Shilling, J., Chen, Q., King, S., Rosenoern, T., Kroll, J., Worsnop, D., McKinney, K., and Martin, S.: Particle mass yield in secondary organic aerosol formed by the dark ozonolysis of α-pinene, Atmos. Chem. Phys., 8, 2073-2088, 2008.

Shiraiwa, M., Li, Y., Tsimpidi, A. P., Karydis, V. A., Berkemeier, T., Pandis, S. N., Lelieveld, J., Koop, T., and Pöschl, U.: Global distribution of particle phase state in atmospheric secondary organic aerosols, Nat. Commun, 8, 1-7, 2017.

Shiraiwa, M. and Seinfeld, J. H.: Equilibration timescale of atmospheric secondary organic aerosol partitioning, Geophys. Res. Lett., 39, 2012.

Tarvainen, V., Hakola, H., Rinne, J., Hellen, H., and Haapanala, S.: Towards a comprehensive emission inventory of terpenoids from boreal ecosystems, Tellus B, 59, 526-534, 2007.

Ulbrich, I. M., Canagaratna, M. R., Zhang, Q., Worsnop, D. R., and Jimenez, J. L.: Interpretation of organic components from positive matrix factorization of aerosol mass spectrometric data, Atmos. Chem. Phys., 9, 2891-2918, 2009.

Vaden, T. D., Imre, D., Beranek, J., Shrivastava, M., and Zelenyuk, A.: Evaporation kinetics and phase of laboratory and ambient secondary organic aerosol, Proc. Natl. Acad. Sci. U. S. A., 108, 2190-2195, 2011.

Wilson, J., Imre, D., Beránek, J., Shrivastava, M., and Zelenyuk, A.: Evaporation kinetics of laboratory-generated secondary organic aerosols at elevated relative humidity, Environ. Sci. Technol., 49, 243-249, 2014.

Virtanen, A., Joutsensaari, J., Koop, T., Kannosto, J., Yli-Pirila, P., Leskinen, J., Makela, J. M., Holopainen, J. K., Poschl, U., Kulmala, M., Worsnop, D. R., and Laaksonen, A.: An amorphous solid state of biogenic secondary organic aerosol particles, Nature, 467, 824-827, 2010.

Yan, C., Nie, W., Aijala, M., Rissanen, M. P., Canagaratna, M. R., Massoli, P., Junninen, H., Jokinen, T., Sarnela, N., Hame, S. A. K., Schobesberger, S., Canonaco, F., Yao, L., Prevot, A. S. H., Petaja, T., Kulmala, M., Sipila, M., Worsnop, D. R., and Ehn, M.: Source characterization of highly oxidized multifunctional compounds in a boreal forest environment using positive matrix factorization, Atmos. Chem. Phys., 16, 12715-12731, 2016.

Yang, L. H., Takeuchi, M., Chen, Y., and Ng, N. L.: Characterization of thermal decomposition of oxygenated organic compounds in FIGAERO-CIMS, Aerosol Science and Technology, doi: 10.1080/02786826.2021.1945529, 2021. 1-22, 2021.

Yasmeen, F., Sauret, N., Gal, J. F., Maria, P. C., Massi, L., Maenhaut, W., and Claeys, M.: Characterization of oligomers from methylglyoxal under dark conditions: A pathway to produce secondary organic aerosol through cloud processing during nighttime, Atmos. Chem. Phys., 10, 3803-3812, 2010.

Yli-Juuti, T., Pajunoja, A., Tikkanen, O. P., Buchholz, A., Faiola, C., Vaisanen, O., Hao, L., Kari, E., Perakyla, O., Garmash, O., Shiraiwa, M., Ehn, M., Lehtinen, K., and Virtanen, A.: Factors controlling the evaporation of secondary organic aerosol from alpha-pinene ozonolysis, Geophys. Res. Lett., 44, 2562-2570, 2017.

Ylisirniö, A., Barreira, L. M. F., Pullinen, I., Buchholz, A., Jayne, J., Krechmer, J. E., Worsnop, D. R., Virtanen, A., and Schobesberger, S.: On the calibration of FIGAERO-tof-CIMS: Importance and impact of calibrant delivery for the particle-phase calibration, Atmos. Meas. Tech., 14, 355-367, 2021.

Ylisirniö, A., Buchholz, A., Mohr, C., Li, Z., Barreira, L., Lambe, A., Faiola, C., Kari, E., Yli-Juuti, T., Nizkorodov, S. A., Worsnop, D. R., Virtanen, A., and Schobesberger, S.: Composition and volatility of secondary organic aerosol (SOA) formed from oxidation of real tree emissions compared to simplified volatile organic compound (VOC) systems, Atmos. Chem. Phys., 20, 5629-5644, 2020.

Zaveri, R. A., Shilling, J. E., Zelenyuk, A., Zawadowicz, M. A., Suski, K., China, S., Bell, D. M., Veghte, D., and Laskin, A.: Particle-phase diffusion modulates partitioning of semivolatile organic compounds to aged secondary organic aerosol, Environ. Sci. Technol., 54, 2595-2605, 2020.

Zhang, Q., Jimenez, J. L., Canagaratna, M. R., Ulbrich, I. M., Ng, N. L., Worsnop, D. R., and Sun, Y.: Understanding atmospheric organic aerosols via factor analysis of aerosol mass spectrometry: A review, Anal. Bioanal. Chem., 401, 3045-3067, 2011.

Zhang, Y., Sanchez, M. S., Douet, C., Wang, Y., Bateman, A. P., Gong, Z., Kuwata, M., Renbaum-Wolff, L., Sato, B. B., Liu, P. F., Bertram, A. K., Geiger, F. M., and Martin, S. T.: Changing shapes and implied viscosities of suspended submicron particles, Atmos. Chem. Phys., 15, 7819-7829, 2015.

Zhao, D. F., Buchholz, A., Tillmann, R., Kleist, E., Wu, C., Rubach, F., Kiendler-Scharr, A., Rudich, Y., Wildt, J., and Mentel, T. F.: Environmental conditions regulate the impact of plants on cloud formation, Nat. Commun, 8, 14067, 2017a.

Zhao, R., Aljawhary, D., Lee, A. K., and Abbatt, J. P.: Rapid aqueous-phase photooxidation of dimers in the α-pinene secondary organic aerosol, Environmental Science & Technology Letters, 4, 205-210, 2017b.

Zhao, R., Kenseth, C. M., Huang, Y., Dalleska, N. F., and Seinfeld, J. H.: Iodometry-assisted liquid chromatography
825 electrospray ionization mass spectrometry for analysis of organic peroxides: An application to atmospheric secondary organic aerosol, Environ. Sci. Technol., 52, 2108-2117, 2018.

Zhao, R., Lee, A. K., and Abbatt, J. P.: Investigation of aqueous-phase photooxidation of glyoxal and methylglyoxal by aerosol chemical ionization mass spectrometry: Observation of hydroxyhydroperoxide formation, J. Phys. Chem. A, 116, 6253-6263, 2012.

830 Zhao, R., Lee, A. K. Y., Soong, R., Simpson, A. J., and Abbatt, J. P. D.: Formation of aqueous-phase α-hydroxyhydroperoxides (α-HHP): Potential atmospheric impacts, Atmos. Chem. Phys., 13, 5857-5872, 2013.
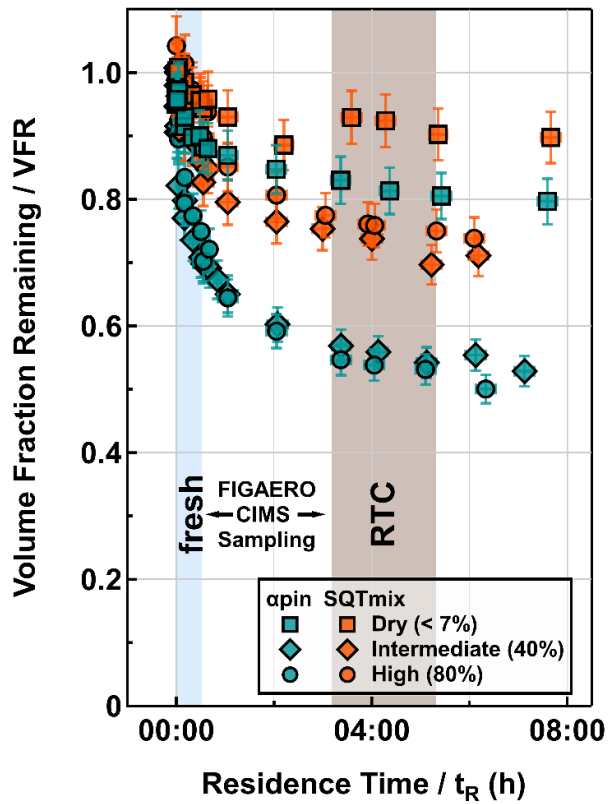
Figure 1. Evapograms for α-pinene (turquoise) and SQTmix (orange) SOA particles under dry (<7%), intermediate RH (40% RH) and high RH (80% RH) conditions. The blue (fresh) and brown (RTC) areas indicate the corresponding sampling periods of FIGAERO-CIMS.
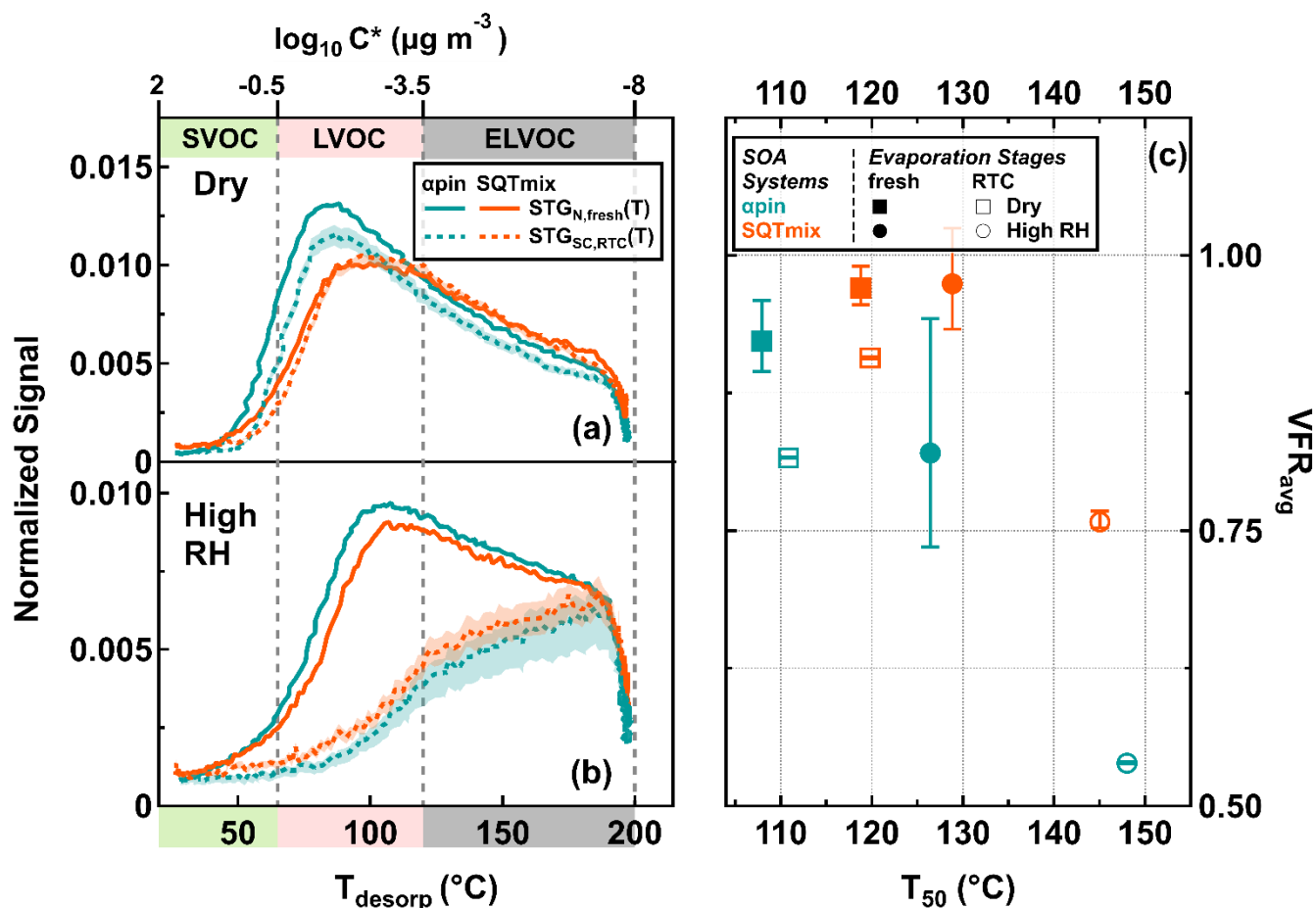
Figure 2. Sum thermograms (STG) (a, b), average volume fraction remaining (VFR$_{avg}$) (c), and median desorption temperature (T$_{50}$) (c) for α-pinene (turquoise) and SQTmix (orange) SOA particles, for dry (RH < 7%; (a)) and high RH (RH 80%; (b)) conditions. Shaded areas indicate the ranges of STG(T) for RTC stages after accounting for changes and uncertainties in average molecular weight and particle density (i.e., $\alpha_{MW_{avg}}$ and $\beta_{\rho_{avg}}$ in Eq. (2). Volatility classes (a, b) are derived from T$_{max}$ − C* calibrations using a set of PEG compounds (Ylisirniö et al., 2021). They are indicated by different color bands on the abscissa using the classification according to Donahue et al. (2012).
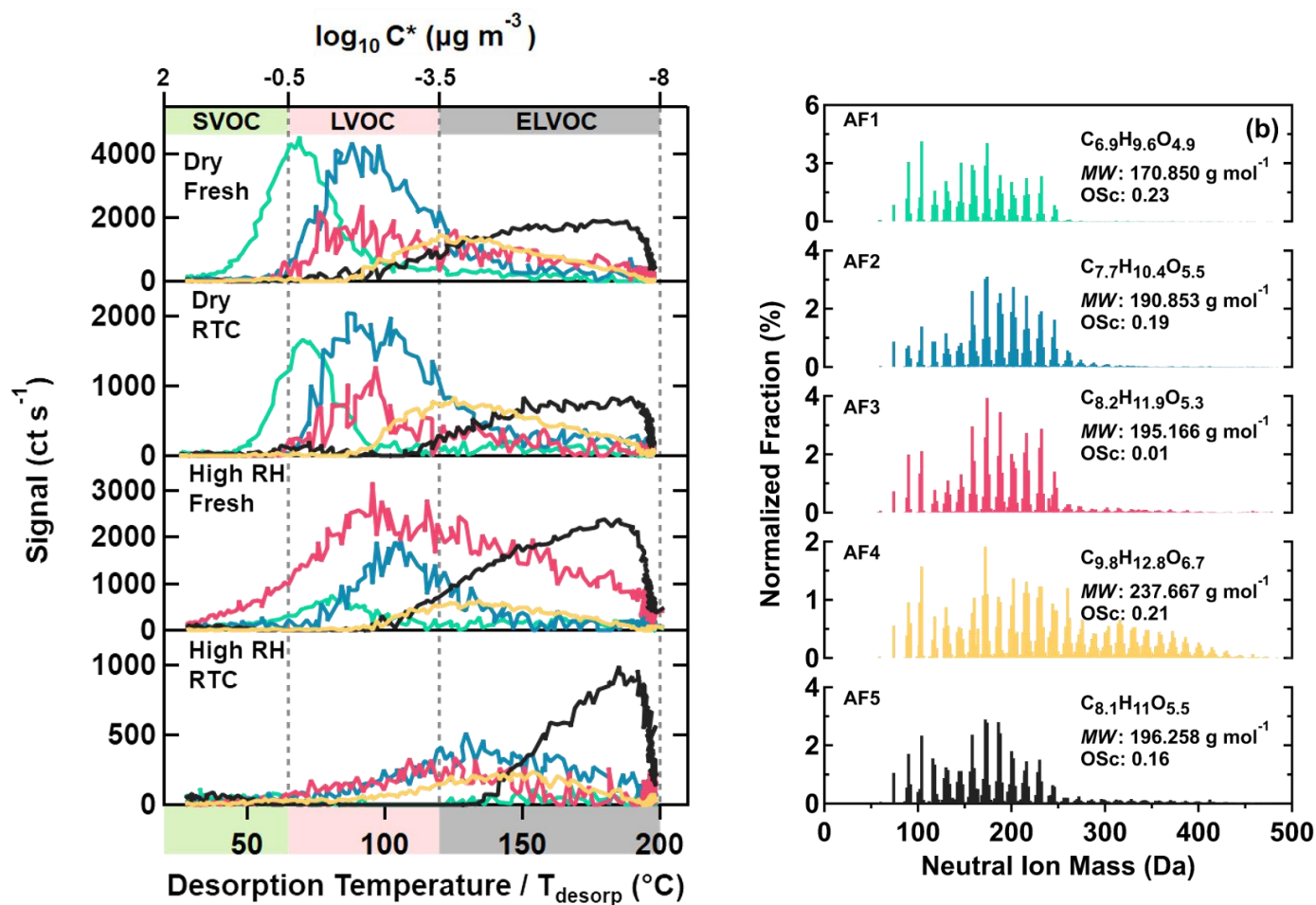
Figure 3. Five main sample factors from an eight-factor PMF solution for α-pinene SOA particles. On the panel (a), factor thermograms are shown with color bands on the abscissa indicating volatility classes. On the panel (b), normalized factor mass spectra are presented with their average molecular composition, molecular weight, and oxidation state. The color code is identical for both panels.
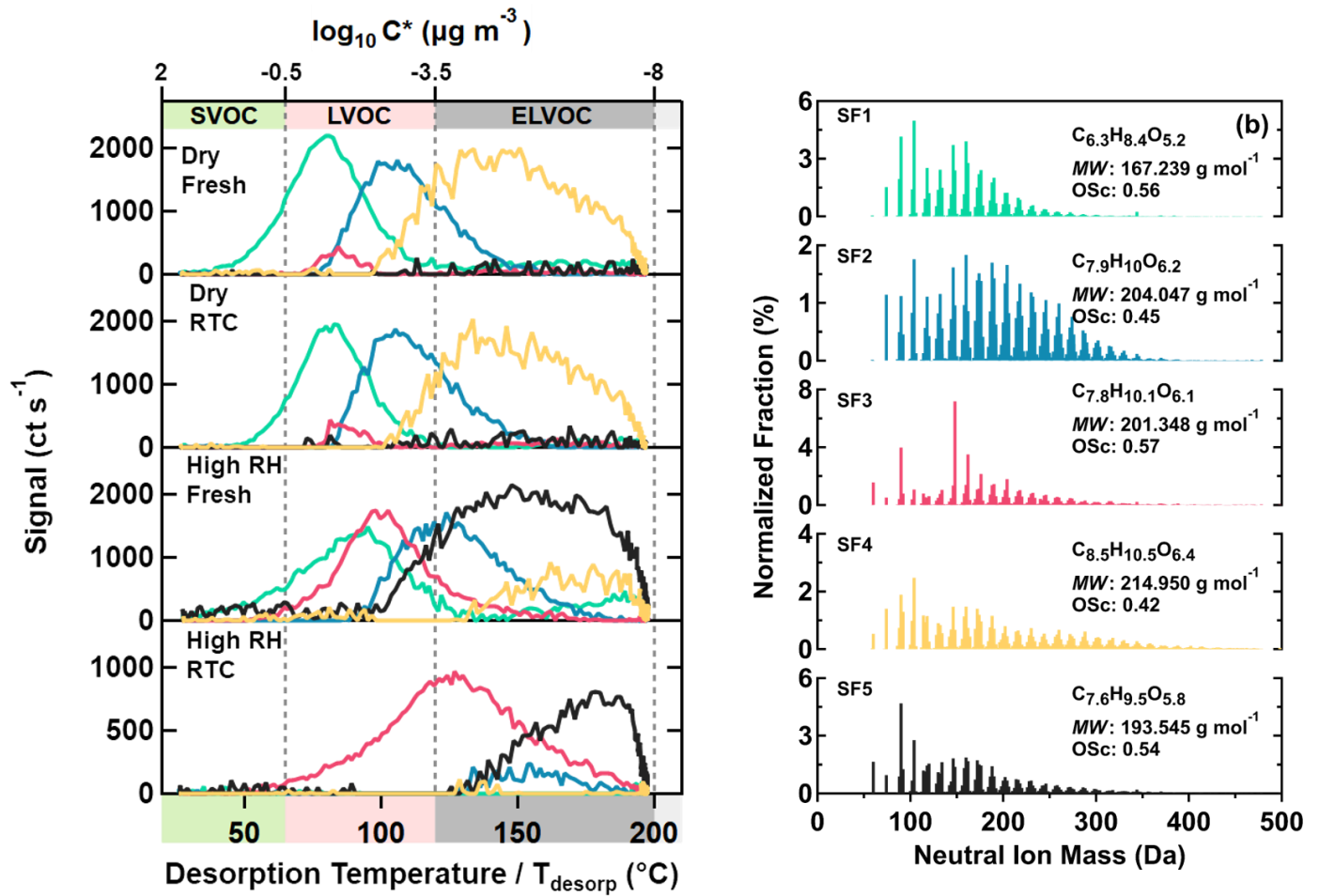
Figure 4. Five main sample factors from a ten-factor PMF solution for SQTmix SOA particles. On the panel (a), factor thermograms are shown with color bands on the abscissa indicating volatility classes. On the panel (b), normalized factor mass spectra are presented with their average molecular composition, molecular weight, and oxidation state. The color code is identical for both panels.
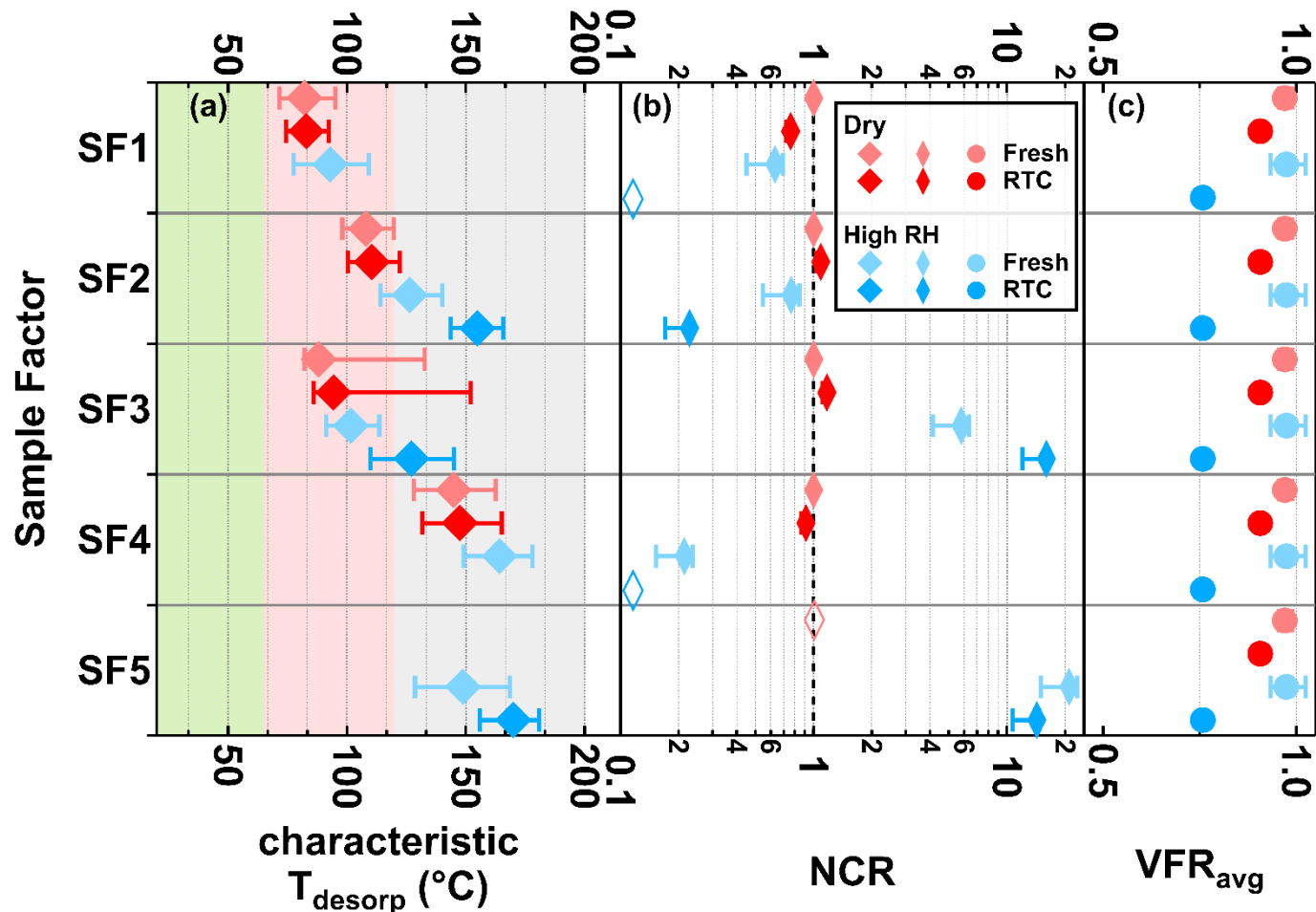
Figure 5. Characteristic desorption temperature (characteristic T_{desorp} with 25th, 50th and 75th percentiles, a), net change ratio (NCR, b) of main sample factors and mean values of volume fraction remaining (VFR$_{avg}$, c) of SQTmix SOA particles at fresh (avg. t_R = 0.25 h) and RTC (avg. t_R = 4.25 h) evaporation stages under dry (red) and high RH (blue) conditions. Background colors in the panel (a) indicate the volatility categories derived from $T_{max} - C^*$ calibrations (green – SVOC; red – LVOC; and grey – ELVOC). Note that values of VFR$_{avg}$ are identical in each row of panel (c). The error bars of NCR represent values accounting for changes in molecular weight and particle density, while those of VFR$_{avg}$ indicates the minimum and maximum values during the FIGAERO sampling time. If the factor thermogram contributes less than 5% to total signals of samples factors and does not exhibit a clear maximum, the corresponding characteristic T_{desorp} values will not be calculated and the NCR will be indicated by an open rhombus closed to 0.1.

Figure 6. Characteristic desorption temperature (characteristic T_{desorp} with 25th, 50th and 75th percentiles, a), net change ratio (NCR, b) of main sample factors and mean values of volume fraction remaining (VFR$_{avg}$, c) of α-pinene SOA particles at fresh (avg. t_R = 0.25 h) and RTC (avg. t_R = 4.25 h) evaporation stages under dry (red) and high RH (blue) conditions. Background colors in the panel (a) indicate the volatility categories derived from $T_{max} - C^*$ calibrations (green – SVOC; red – LVOC; and grey – ELVOC). Note that values of VFR$_{avg}$ are identical in each row of panel (c). The error bars of NCR represent values accounting for changes in molecular weight and particle density, while those of VFR$_{avg}$ indicates the minimum and maximum values during the FIGAERO sampling time. If the factor thermogram contributes less than 5% to total signals of samples factors and does not exhibit a clear maximum, the corresponding characteristic T_{desorp} values will not be calculated and the NCR will be indicated by an open rhombus closed to 0.1.

Evaporation of Sesquiterpene-mixed SOA Particles

Size Change
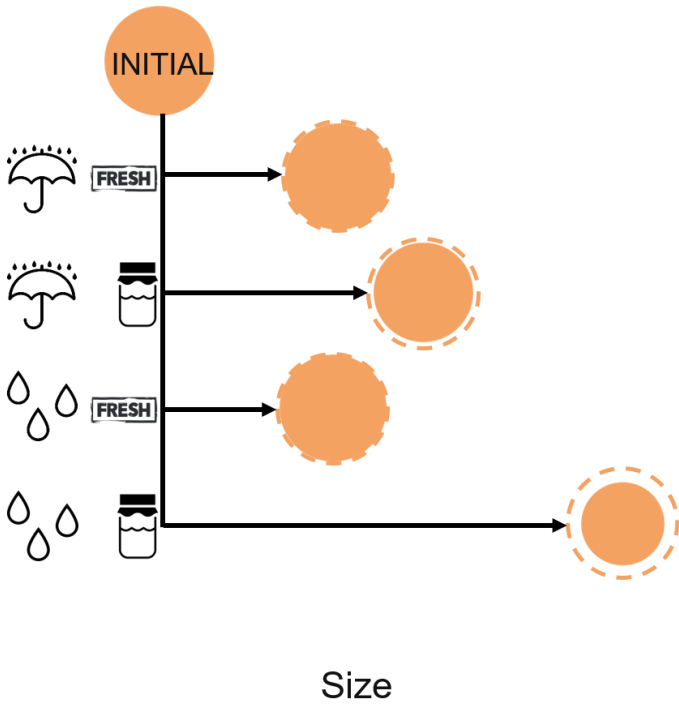
Molecular-level Change

Size

Fraction (%)

880

For Key Figure Only